Received: 13 February 2024 | Revised: 29 July 2024 | Accepted: 22 August 2024

IET Renewable Power Generation

DOI: 10.1049/rpg2.13099

The Institution of Engineering and Technology WILEY

ORIGINAL RESEARCH

Comprehensive assessment of voltage and current source PV-based modular multilevel converters

Marzio Barresi | **Luigi Piegari** | **Riccardo Scalabrin**

Department of Electronics, Informatics and Bioengineering, Politecnico di Milano, Milan, Italy

Correspondence
Riccardo Scalabrin, Department of Electronics, Informatics and Bioengineering, Politecnico di Milano, P.za Leonardo da Vinci 32, Milan, Italy.
Email: riccardo.scalabrin@polimi.it

Abstract

Recently, modular multilevel converters (MMCs) gained popularity for the grid integration of photovoltaic (PV), due to their many advantages, including low total harmonic distortion, high control flexibility, and distributed maximum power point (MPP) tracking capability. Two distinguished families of MMCs exist: voltage source and current source. Voltage source MMCs are mostly studied, but current source MMCs offer advantages under certain operating conditions. This article compares voltage and current source MMCs, for PV integration. To this aim, several key indicators are identified: number of components, energy stored in passive elements, semiconductor power rating, and the number of MPP trackers. The results of the analysis, performed in MATLAB©, show that for a fixed number of output voltage levels, power rating, and switching frequency, voltage source MMCs have simpler control and higher number of MPP trackers. In contrast, current source MMCs minimize the semiconductor power rating, the number of components and the energy stored in passive elements. Regarding efficiency, in the analyzed case study, voltage source MMCs perform better under both homogeneous and non-homogenous irradiance conditions. This article provides a tool to select the optimal solution based on the required target (e.g. efficiency, energy storage etc.), given the specific characteristics of the application.

1 | INTRODUCTION

In recent years, researchers, companies, and authorities have employed significant resources for the study and development of innovative technologies and solutions for the decarbonization of the energy production sector, directing a steadily growing interest towards renewable energy sources (RES), such as photovoltaic (PV) [1], to reduce greenhouse gas emissions. However, the unpredictability of such RES poses significant challenges for grid management, leading to the necessity to utilize flexible interfaces for performing their integration within the power grid [2]. A PV plant consists of several PV modules, which are suitably connected in series and in parallel to constitute arrays. Those arrays are then interfaced with the AC grid, typically by employing a power electronics-based power conversion system (PCS). As the amount of power that the PV system is able to deliver strongly depends on the modules irradiance and temperature operating conditions [3], maximum power point tracking (MPPT) algorithms are implemented for the PCS control - either on the main power converter or by means of additional DC-DC stages - thus ensuring the injection of the maximum available power into the grid [4].

The existing literature addresses many different realizations of a PCS interface for PV plants. Traditional solutions require a single-stage two-level three-phase voltage source converter (VSC) [5], also implementing a centralized MPPT function. Alternatively, an additional intermediate DC-DC stage can be adopted to integrate the PV modules. In this solution, the DC-DC converter is responsible for boosting the voltage and perform the MPPT function. This additional stage can interface with the whole PV system, achieving a centralized approach, or, alternatively, several DC-DC stages can be used, one for each subgroup of the PV plant, achieving a distributed approach [6]. Indeed, the maximum power point (MPP) of the PV system is not unique, particularly in the case of non-homogeneous irradiance conditions [7]. By adopting a distributed maximum power

point tracking (DMPPT) it becomes possible to track each local MPP, consequently enhancing the overall efficiency of the PV plant. Despite their simplicity, two-level VSCs require bulky filters and dedicated transformers for grid connection at high voltages. In this context, PCS based on modular multilevel converters (MMCs) provide significant advantages over previous ones: the modular structure of MMCs enables a direct interface of the PV arrays, without requiring additional conversion stages for boosting the voltage of the modules, while at the same time providing the possibility to implement DMPPT algorithms [8]. Moreover, increasing the number of levels of the output waveform considerably decreases its total harmonic distortion (THD), therefore reducing filtering requirements [9].

An MMC consists of the repetitive interconnection of many power electronics blocks, herein referred to as submodules (SMs). In the literature, two main families of MMCs can be distinguished, namely voltage source and current source MMCs. Their fundamental difference lies in the power source connected on the DC side of the converter, operating either as a constant voltage or current source, respectively, as well as on several other structural and control aspects which are deeply analyzed in this work.

Considering voltage source MMCs solutions, a two-stage neutral point clamped converter is proposed in [10]. However, the necessity to realize a common DC link actually limits the possibility to implement a DMPPT, hence negatively affecting the efficiency of the PCS under non-homogeneous irradiance conditions. The same issue is also shared by flying capacitor voltage source MMC topologies [11]. The authors of [12] and [13] propose a single-phase cascaded H-bridge topology with MPPT capability enabling the direct connection of the PV system with a single-phase low voltage AC grid. Regarding large-scale plants, three-phase cascaded H-bridge solutions are preferred, with studies dealing with both star and delta-connected cascaded H-bridge topologies [14–16]. Another well-known voltage source MMC topology is the double star chopper cell (DSCC) MMC. Several examples of DSCC PCS interfaces for the grid integration of PV plants are present in the literature, directly interconnecting the PV arrays to the converter SMs [17, 18] or using additional flyback [19] or dual-active bridge [20] DC-DC stages to provide galvanic isolation. In this converter topology, internal power mismatches are typically managed injecting opportune components of the circulating currents [18, 20].

Several viable solutions can be found in the literature also concerning current source converters. The authors of [21] propose the adoption of a single stage current source converter with centralized MPPT capability for the grid interface of a small scale PV system. A similar solution is proposed also by [22], where the MPPT function is distributed and implemented by means of additional DC-DC conversion stages. A further development is introduced by the authors of [23], employing an additional switch to enhance the inherent voltage boost behavior of the classic current source converter interface [24]. Considering current source MMCs, the grid integration of a large-scale PV plant can be realized with a current source cascaded H-bridge, as done in [25]. At last, [26] shows the adoption of a modular multilevel current source topology comprising several three-phase SMs connected in parallel to each other. In this solution, each converter SM can be individually controlled to inject the maximum power of the integrated PV arrays. Therefore, compared to the DSCC MMC, no additional current components should be generated.

The comparison between two different converter topologies with different control strategies is not straightforward unless specific criteria and constraints are fixed. In light of these considerations, the aim of this work is to extend and finalize the comparison between voltage and current source MMCs for PV integration first introduced in [27]. The outcomes of this analysis provide engineers and power electronics designers with useful insights about which solution maximizes the required targets (e.g. efficiency, costs etc.) according to the specific characteristics of the application. Among the several solutions present in the literature, the topologies proposed in [17] and [26] were selected. This choice was made because these architectures minimize the number of components, as they do not require additional conversion stages within the converter SMs.

The article is organized as follows: after briefly introducing the two converter topologies in Section 2, Section 3 summarizes the results of [27] for the count of the number of SMs, active and passive components, number of PI regulators, and MPP trackers for two converters having the same number of levels of the output waveforms. The energetic comparison between the two solutions is finalized in Section 4 with the addition of the power ratings of the semiconductors. Moreover, the analysis takes into account the effects of non-homogeneous irradiance. Specifically, for the modular multilevel voltage source (MMVS), the occurrence of irradiance imbalances leads to the circulation of additional AC and DC current components, thus impacting both losses and the ratings of active and passive components. On the other hand, this is not the case for current source MMCs, as for the topology under analysis, the SMs of the converter operate independently from each other even in the presence of non-homogeneous irradiance conditions. Finally, Section 5 proposes a case study for the grid integration of a 50 kW PV plant and compares the efficiency of the two MMCs considering for both homogeneous and non-homogeneous irradiance conditions. Eventually, Section 6 concludes the article.

2 | MODULAR MULTILEVEL CONVERTERS TOPOLOGIES

As anticipated in Section 1, the aim of this work is to provide to power electronics engineers a specific framework for comparing two MMCs topologies, namely, a voltage source and a current source MMC, presented in [17] and [26], respectively. This is performed by fixing specific constraints, both structural and energetic (i.e. on the number of output levels or on the converter rating). The comparison provides fruitful insights to the designer, helping in understanding the advantages and disadvantages of the two topologies under different operating conditions (e.g. in case of homogeneous or non-homogeneous irradiance of the PV arrays).

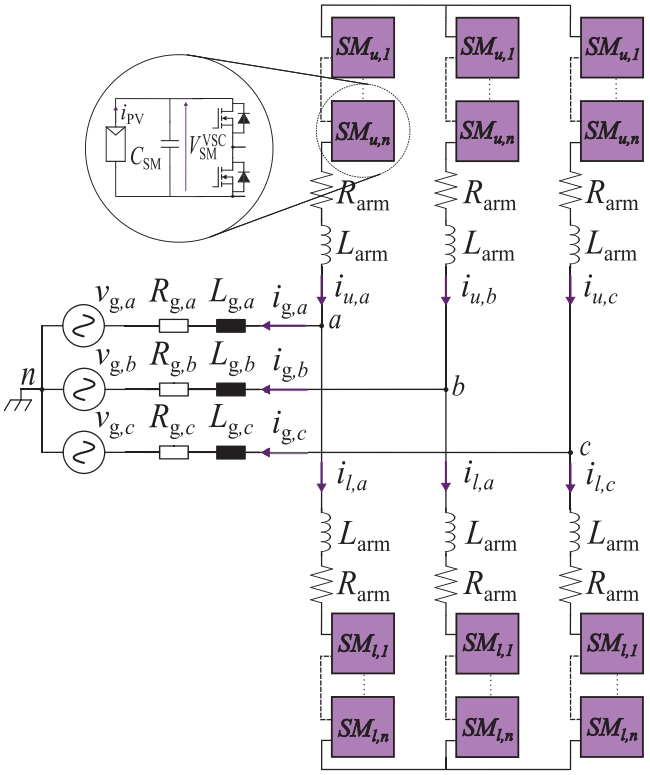

FIGURE 1 Voltage source MMC.

2.1 | Voltage source MMC

The structure of the MMVS converter shown in Figure 1 consists of the series connection of n half-bridge SMs and an inductor with inductance L_{arm} and stray resistance R_{arm}, forming an arm. The interconnection of the upper and lower arms, identified in Figure 1 by subscripts u and l, respectively, constitutes a leg. The overall MMVS comprises three legs, one for each phase of the converter. Each SM integrates a PV array, together with a submodule capacitor of capacitance C_{SM}, aimed at smoothing the SM voltage ripple.

The MMVS is then interfaced with the power grid by means of an inductive filter. Considering also the grid inductance L_g, the equivalent output inductance of the converter is $L_g + L_{arm}/2$ [17].

Concerning the modulation techniques, several different solutions can be found in the literature [28]. For the scope of this work, a modulation scheme able to provide $2n + 1$ voltage levels has been considered (e.g. phase-disposition PWM), to better exploit the converter capabilities in terms of number of levels. Alternative modulation strategies provide only $n + 1$ levels at the output voltage terminals. Regarding the MMVS control strategy, the same solution adopted in [20] has been taken into account for the evaluation of the control complexity. Indeed, compared to [17], which proposes managing internal converter mismatches with redundant SMs, [20] exploits circulating currents. Since this strategy is more common and does not require additional components, it was preferred to achieve a fair comparison between the converters.

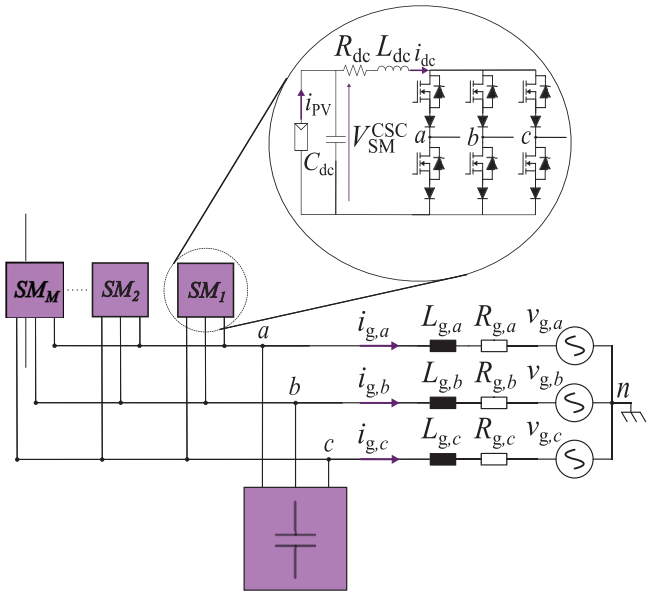

FIGURE 2 Current source MMC.

2.2 | Current source MMC

The overall structure of the current source MMC is shown in Figure 2. Similarly to the voltage source MMC, the PV arrays are directly connected to the SM through a parallel capacitor (C_{dc}) and an inductor (L_{dc}) with stray resistance R_{dc}. A three-phase capacitor bank filters the output current waveform at the connection point with the AC grid. Unlike the voltage source MMC, the SMs of this converter have three-phase outputs. Moreover, depending on the application, particularly on the requirement for either unidirectional or bidirectional current flow, the SMs can be realized using different combinations of switches [29]. Referring to the target application of this work (i.e. the grid integration of a PV system), power only flows from the PV arrays to the grid, and the current flowing in the switches is unidirectional. Therefore, current source MMCs can be further subdivided into two subgroups: reverse-blocking modular multilevel current source (MMCS-RB) converters have SMs realized with six reverse-blocking (RB) switches, such as IGBTs with RB capability, while non reverse-blocking modular multilevel current source (MMCS-NRB) converters use non reverse-blocking (NRB) switches (such as SiC MOSFETs or IGBTs) with series diodes, as shown in Figure 2. In the first case, six power electronics components are needed to realize each one of the M SMs, while in the latter case twelve power electronics components *per submodule* are required. For the sake of coherence, also in this case, a modulation scheme able to provide $2M + 1$ current levels has been applied (i.e. phase shift carrier PWM), as for the voltage source MMC. It is worth noting that, in case of non-homogeneous irradiance condition, the DC current of each SM might differ. Nevertheless, each SM is controlled to operate with a unitary modulation index to extract its maximum available power. Regarding the converter control, a dedicated AC current PI regulator is considered for each submodule, instead of using a centralized controller as in [26], enabling the

independent operation of each SM. This choice increases the control complexity, as the number of PI regulators is higher, but it improves the MPP tracking performances, enhancing the efficiency of the PCS, especially in case of non-homogeneous irradiance conditions.

3 | CONVERTERS STRUCTURAL COMPARISON

Referring to the results presented in [27], the structural comparison between the two MMC topologies is developed by fixing a constraint on the *number of voltage or current levels* provided at the output phase terminals by each converter. Hence, it is assumed that the two converters provide the same number of levels N_{lev} of the output voltage or current waveforms, respectively. Moreover, by assumption, both converters have the same power rating and switching frequency.

Given these constraints, the passive and active electrical components, and control elements (i.e. inductors, capacitors, switches, diodes, PI regulators, and MPP trackers) needed to realize a MMVS, an MMCS-RB, and an MMCS-NRB converter are counted and compared.

Due to the adopted modulation schemes, the total number of SMs of the two converters can be directly related to N_{lev}. For the voltage source MMC, it holds that $N_{\text{lev}} = 2n + 1$, while for the current source MMC, N_{lev} equals $2M + 1$. However, while for the current source MMC, M represents the total number of SMs of the converter, for the voltage source MMC, n is the number of SMs in each arm. Hence, for a coherent comparison, the total number of SMs N of the voltage source MMC has to be considered. Indeed, N_{lev} and N are related as:

$$N_{\text{lev}} = \frac{N}{3} + 1. \tag{1}$$

Therefore, the total number of submodules (i.e. N and M) can be expressed as a function of N_{lev}:

$$N = 3(N_{\text{lev}} - 1), \tag{2}$$

$$M = \frac{1}{2}(N_{\text{lev}} - 1). \tag{3}$$

Figure 3 highlights that voltage source MMCs require more SMs than their current source counterpart. This is due to the different SMs structure, and in particular, it is related to the three-phase nature of the SMs of the current source MMC. Indeed, while the SMs of the voltage source MMC can only modify the voltage of each leg—and thus, of each phase—the SMs of the current source MMC are able to set the current levels on the three output phases of the converter.

On the other hand, the SMs of a MMVS are built using just two switches, while at least six power electronics components are required for the SMs of a current source MMC (i.e. six for a MMCS-RB, six plus six series diodes for a MMCS-NRB). Therefore, Figure 4 puts under comparison the number of switches, diodes, inductors, and capacitors required by the two converters,

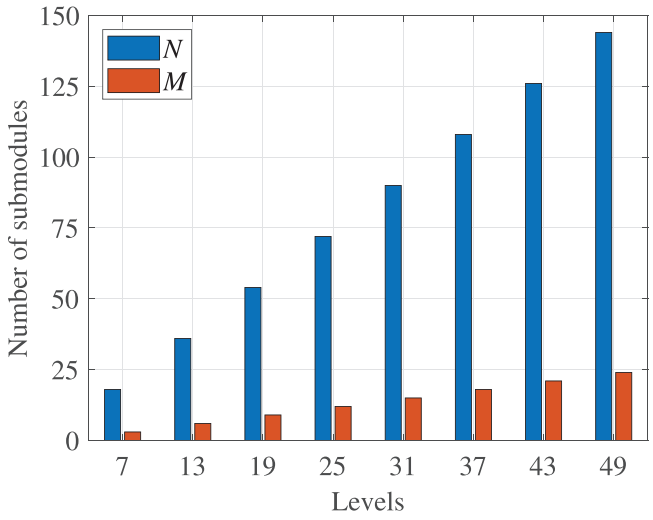

FIGURE 3 Number of SMs, given N_{lev}.

given a fixed number of levels and considering both MMCS-RB and MMCS-NRB sub-topologies. It can be observed that:

$$\begin{aligned} N_{\text{switches}}^{\text{MMCS-RB}} &= N_{\text{switches}}^{\text{MMCS-NRB}} = 3(N_{\text{lev}} - 1), \\ N_{\text{diodes}}^{\text{MMCS-RB}} &= 0; N_{\text{diodes}}^{\text{MMCS-NRB}} = 3(N_{\text{lev}} - 1), \\ N_{\text{switches}}^{\text{MMVS}} &= 6(N_{\text{lev}} - 1), \end{aligned} \tag{4}$$

where:

- $N_{\text{switches}}^{\text{MMCS-RB}}$ and $N_{\text{diodes}}^{\text{MMCS-RB}}$ are the number of switches and diodes required by the MMCS-RB, respectively.
- $N_{\text{switches}}^{\text{MMCS-NRB}}$ and $N_{\text{diodes}}^{\text{MMCS-NRB}}$ are the number of switches and diodes required by the MMCS-NRB, respectively.
- $N_{\text{switches}}^{\text{MMVS}}$ represents the number of switches required by the MMVS.

Given N_{lev}, a current source MMC requires half the number of switches of a voltage source MMC. However, for the MMCS-NRB, the number of power electronics components is equal to the MMVS converters since the MMCS-NRB requires connecting a diode in series to each switch. Instead, for the same number of output levels, the MMCS-RB requires half the components than the MMVS.

Concerning the passive components, a voltage source MMC requires fewer inductors, that is, 6 (one for each arm), independently of N_{lev}, while current source MMCs require one inductor *per submodule*, that is, M. On the other hand, voltage source MMCs require many more DC side capacitors, equal to the total number of SMs, that is, N. Indeed, the voltage source MMCs have more SMs for a fixed number of levels, N_{lev}. Instead, the current source MMCs require one capacitor *per submodule* plus 3 output filter capacitors, thus, in total $M + 3$. In Figure 4, the analysis of the number of components is reported. Specifically, Figure 4c summarizes the structural comparison, considering the total number of active and passive components together. MMVS converters require the highest number of components;

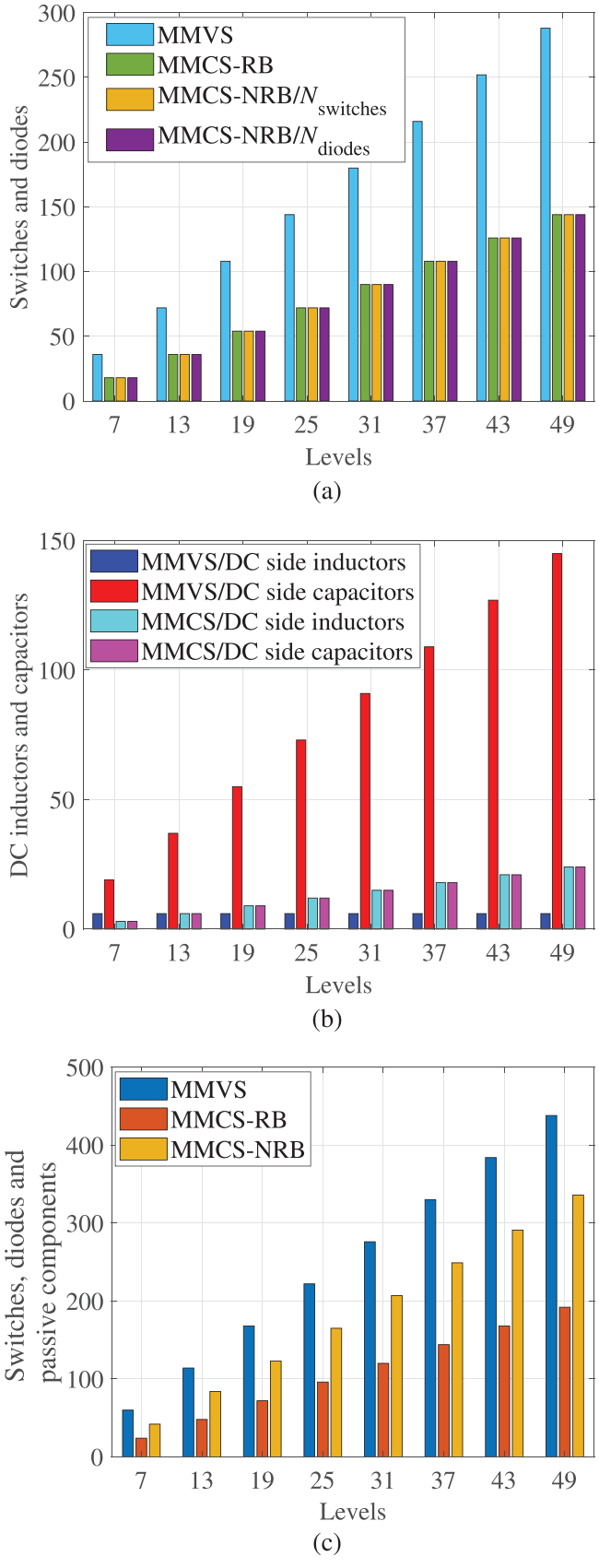

FIGURE 4 (a) Number of switches and diodes; (b) number of passive components; (c) total number of electrical components.

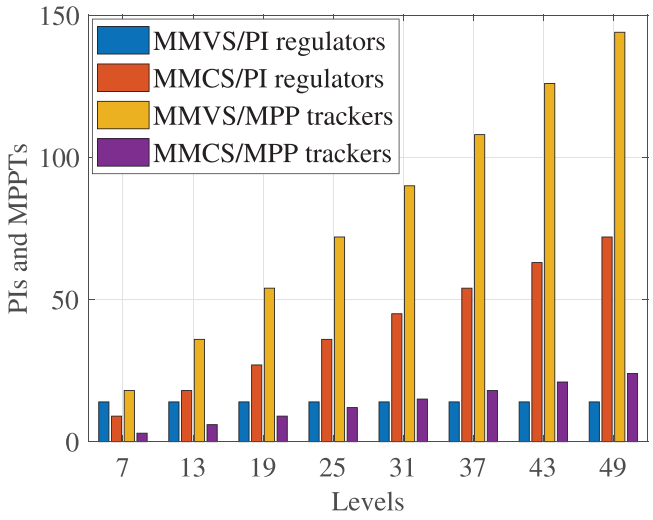

FIGURE 5 Number PI regulators and MPP trackers.

MMCS-RB converters the lowest, with MMCS-NRB converters in between.

At last, the plot of Figure 5 provides insights into the number of PI regulators and MPP trackers, to compare the control complexity and the possibility to track different MPPs of the plant in case of non-homogeneous irradiance conditions. Concerning the number of PI regulators, voltage source MMCs perform better than current source MMCs, especially as N_{lev} increases. The reason is that the same number of PI regulators (independently of the number of levels) are required for the control, while for the current source MMCs, since independent control of each SM is considered, the number of PI regulators increases with the number of levels. In the voltage source MMCs, the control algorithm is based on the grid and circulating controller [20]. The grid controller requires two PIs for controlling direct and quadrature current components, and one external regulator for defining the direct current components related to the maximum power of the PV plant. The circulating controller requires controlling $\alpha\beta 0$ components of the AC and DC circulating currents, and 5 external regulators (three for the AC and two for the DC components) for defining the reference circulating currents. In the current source MMCs, three PI regulators *per submodule* are needed. Two PIs for controlling direct and quadrature current components, and one external regulator for defining the direct current components related to the maximum power of the PV array integrated in the SM. Regarding the number of MPP trackers, in both converters it increases proportionally with N_{lev}. However, since it is equal to the number of SMs, that is, N or M according to the converter topology, in the current source MMCs increases in a slower way with respect to voltage source MMCs. Indeed, the voltage source MMCs have more SMs than current source MMCs, given the same number of levels. This aspect, on one side, is positive since the power production of the PV plant can be improved, since a more distributed approach is achieved, while on the other side increase the control complexity.

4 | ENERGETIC COMPARISON

In [27], a comparison of the total energy stored by all the inductive and capacitive elements of the two MMC topologies was performed, considering, however, only homogeneous irradiance conditions. In this work, this analysis was extended and reformulated considering non-homogeneous irradiance of the PV plant. Indeed, in this scenario the converters operation differ significantly. For instance, for the MMVS, it is required to generate additional current components to ensure delivering balanced power to the grid. In addition, also the power semiconductor ratings are computed and included in the comparison, considering the MMVS and both MMCS-RB and MMCS-NRB converters.

The energetic analysis is performed in such a way as to express all the quantities according to the rated values of the system. In a rotating *dq*-axes reference frame, considering the preservation of the amplitude of the electrical quantities, the rated active and reactive power exchanged with the grid are:

$$P_{\mathrm{ac}} = \frac{3}{2}(v_{\mathrm{g,d}} i_{\mathrm{g,d}} + v_{\mathrm{g,q}} i_{\mathrm{g,q}}), \tag{5}$$

$$Q_{\mathrm{ac}} = \frac{3}{2}(v_{\mathrm{g,q}} i_{\mathrm{g,d}} - v_{\mathrm{g,d}} i_{\mathrm{g,q}}), \tag{6}$$

where:

- P_{ac}, Q_{ac} are the active and reactive power.
- $v_{\mathrm{g,d}}$, $i_{\mathrm{g,q}}$ are the *d*-axis voltage and current.
- $v_{\mathrm{g,q}}$, $i_{\mathrm{g,q}}$ are the *q*-axis voltage and current.

A decoupled control of active and reactive power is achieved using a phase locked loop (PLL), which locks the phase of the AC line-to-ground grid voltage, fixing $v_{\mathrm{g,q}} = 0$ [30]. Therefore, the rated active and reactive power, P^{r}_{ac} and Q^{r}_{ac}, respectively, can be expressed as:

$$P^{\mathrm{r}}_{\mathrm{ac}} = \frac{3}{2} v^{\mathrm{r}}_{\mathrm{g,d}} i^{\mathrm{r}}_{\mathrm{g,d}}, \tag{7}$$

$$Q^{\mathrm{r}}_{\mathrm{ac}} = -\frac{3}{2} v^{\mathrm{r}}_{\mathrm{g,d}} i^{\mathrm{r}}_{\mathrm{g,q}}, \tag{8}$$

where $v^{\mathrm{r}}_{\mathrm{g,d}}$ is the rated value of the *d* component of the grid voltage, and $i^{\mathrm{r}}_{\mathrm{g,d}}$, and $i^{\mathrm{r}}_{\mathrm{g,q}}$ are the rated values of the *dq* components of the output converter currents.

If active power losses are neglected, then $P_{\mathrm{dc}} \approx P_{\mathrm{ac}}$, where P_{dc} is the power comprehensively produced by the PV plant and injected by the SMs.

4.1 | Voltage source MMC

4.1.1 | Capacitive and inductive energy

The expression of the total capacitive energy $E_{\mathrm{c,vsc}}$ stored by the capacitors in the SMs is:

$$E_{\mathrm{c,vsc}} = \frac{N}{2} C_{\mathrm{SM}} V^{\mathrm{VSC,r}^2}_{\mathrm{SM}}. \tag{9}$$

Considering (7), the rated SM voltage, $V^{\mathrm{VSC,r}}_{\mathrm{SM}}$, is given by:

$$V^{\mathrm{VSC,r}}_{\mathrm{SM}} = \frac{2v^{\mathrm{r}}_{\mathrm{g,d}}}{n} = 8\frac{P^{\mathrm{r}}_{\mathrm{ac}}}{N i^{\mathrm{r}}_{\mathrm{g,d}}}, \tag{10}$$

where $n = N/6$ is the number of SMs in each converter arm. It is worth noting that (10) was derived considering that each converter arm should be able to synthesize at least double of the rated grid voltage. Even though a margin on the SM voltage related to power regulation or PV sizing is typically considered, for the sake of simplicity, it was neglected. Additionally, the submodule capacitor could be sized according to [31] as:

$$C_{\mathrm{SM}} \approx \frac{P^{\mathrm{r}}_{\mathrm{ac}}}{2\pi f \xi^{\mathrm{rip}}_{\mathrm{sm,vsc}} \sqrt{(6-4\sqrt{3})\left(\xi^{\mathrm{rip}^2}_{\mathrm{sm,vsc}} - 4\right)} N V^{\mathrm{VSC,r}^2}_{\mathrm{SM}}}, \tag{11}$$

where:

- f is the frequency of the grid.
- $\xi^{\mathrm{rip}}_{\mathrm{sm,vsc}} \in (0, 1]$ is fixed by the designer as a degree of freedom and it represents the allowed voltage ripple of $V^{\mathrm{VSC,r}}_{\mathrm{SM}}$.

The SM capacitor expression was derived assuming the converter is exchanging solely active power with the grid. Eventually, substituting (11) in (9), the total capacitive energy of the MMVS becomes:

$$E_{\mathrm{c,vsc}} = \frac{P^{\mathrm{r}}_{\mathrm{ac}}}{4\pi f \xi^{\mathrm{rip}}_{\mathrm{sm,vsc}} \sqrt{(6-4\sqrt{3})\left(\xi^{\mathrm{rip}^2}_{\mathrm{sm,vsc}} - 4\right)}}. \tag{12}$$

It is interesting to highlight that $E_{\mathrm{c,vsc}}$ does not depend on the structural characteristics of the voltage source MMC, that is, on the number of SMs.

Concerning the total inductive energy stored in the arm inductors, it is strictly related to the maximum arm current, $i^{\mathrm{max}}_{\mathrm{arm}}$, as:

$$E_{\mathrm{l,vsc}} = \frac{6}{2} L_{\mathrm{arm}} i^{\mathrm{max}^2}_{\mathrm{arm}}. \tag{13}$$

The arm current, $i_{\mathrm{u},k}$ or $i_{\mathrm{l},k}$, for the upper or lower arm, respectively, depends on two main components, that is, the output converter currents, $i_{\mathrm{g,k}}$, and the circulating currents, $i_{\mathrm{circ},k}$. Considering Figure 1, the general expression of the arm current, $i_{\mathrm{arm},k}$, can be written as:

$$i_{\mathrm{arm},k} = \pm\frac{i_{\mathrm{g},k}}{2} + i_{\mathrm{circ},k}. \tag{14}$$

The grid currents are related to the active and reactive power exchanged with the grid, while the circulating currents are additional current components opportunely injected into the

converter to manage its internal energy [20]. In particular, in the case of non-homogeneous irradiance conditions, the fundamental AC circulating component aims at managing the power mismatches among the upper and lower arms, while the DC component manages the power mismatches among the converter legs. In this way, each arm can operate at the MPP, optimizing the power production of the PV plant. It follows that the worst-case scenario to be considered for determining the energy stored by the inductive components is the one in which these aforementioned current components are the highest. This occurs in the presence of strongly non-homogeneous irradiance conditions. Assuming that the maximum power output of one arm is equal to $P_{\mathrm{ac}}^{\mathrm{r}}/6$, it is possible to demonstrate that the highest arm current occurs when [32]:

$$\begin{aligned} P_{\mathrm{d},k} &= P_{u,k} - P_{l,k} = \pm P_{\mathrm{ac}}^{\mathrm{r}}/6 \quad && k \in a, b, c \\ P_{\mathrm{d},y} &= P_{\mathrm{d},z} = -P_{\mathrm{d},k} && y \neq k, z \neq y \neq k \end{aligned}, \tag{15}$$

where $P_{\mathrm{d},k}$ is the active differential power, while $P_{u,k}$ and $P_{l,k}$ are the powers produced by the upper and lower arm of the k-th phase, respectively. In this scenario, only extreme imbalances among the arms are present, requiring injecting solely the AC components of the circulating current. The PV system is producing half of the rated power, that is, $P_{\mathrm{ac}}^{\mathrm{r}}/2$, and the maximum value of the circulating current is given by (see Appendix):

$$i_{\mathrm{circ}}^{\max} = \frac{\sqrt{21} i_{\mathrm{g,d}}^{\mathrm{r}}}{12}. \tag{16}$$

Therefore, under this extreme arm unbalanced condition, the maximum arm current is given by:

$$i_{\mathrm{arm}}^{\max} = \left| \frac{i_{\mathrm{g,d}}}{2} \right| + i_{\mathrm{circ}}^{\max} = \frac{i_{\mathrm{g,d}}^{\mathrm{r}}}{4} + \frac{\sqrt{21} i_{\mathrm{g,d}}^{\mathrm{r}}}{12}. \tag{17}$$

It is worth noting that, even if half of the rated power is injected into the grid, consequently decreasing the contribution of the term $i_{\mathrm{g,d}}$, the additional circulating component increases the arm current, making the extreme arm unbalanced condition more critical than the case in which the plant maximum power is exchanged with the grid.

After determining the maximum arm current, the arm inductor should be designed. The scope of the arm inductors is to smooth the ripple of the arm currents, Δi_{arm}, which equals:

$$\Delta i_{\mathrm{arm}} = \xi_{\mathrm{arm}}^{\mathrm{rip}} i_{\mathrm{arm}}^{\max} = \frac{\Delta V_{L\mathrm{arm}}}{L_{\mathrm{arm}} f_{\mathrm{s}}}, \tag{18}$$

where f_{s} is the converter switching frequency and $\xi_{\mathrm{arm}}^{\mathrm{rip}} \in (0, 1]$ represents the maximum allowed arm current ripple, and it is a degree of freedom fixed by the designer. Additionally, the maximum voltage ripple across the inductor, $\Delta V_{L\mathrm{arm}}$, it is equal to rated SM voltage. The latter was defined in (10) as:

$$\Delta V_{L\mathrm{arm}} = V_{\mathrm{SM}}^{\mathrm{VSC,r}} = 8 \frac{P_{\mathrm{ac}}^{\mathrm{r}}}{N i_{\mathrm{g,d}}^{\mathrm{r}}}. \tag{19}$$

Consequently, the sizing of the arm inductance, L_{arm}, results:

$$L_{\mathrm{arm}} = \frac{\Delta V_{L\mathrm{arm}}}{\Delta i_{\mathrm{arm}} f_{\mathrm{s}}} = \frac{8 P_{\mathrm{ac}}^{\mathrm{r}}}{\xi_{\mathrm{arm}}^{\mathrm{rip}} N {i_{\mathrm{g,d}}^{\mathrm{r}}}^2 f_{\mathrm{s}}} \left(\frac{12}{3 + \sqrt{21}} \right). \tag{20}$$

Lastly, substituting (20) and (17) in (13), the total inductive energy stored in the arm inductors of the voltage source MMC is computed as:

$$E_{\mathrm{l,vsc}} = \frac{\left(6 + 2\sqrt{21}\right) P_{\mathrm{ac}}^{\mathrm{r}}}{f_{\mathrm{s}} N \xi_{\mathrm{arm}}^{\mathrm{rip}}}. \tag{21}$$

It is worth noting that, in the considered converter topology, the arm inductor acts also as a filter for the converter output currents.

4.1.2 | Power semiconductors rating

Let us now compute the power semiconductor rating of the voltage source MMC. It is worth including this quantity in the energetic comparison, as it strongly relates to the cost of the active switches. Also in this case, the power semiconductor rating is computed according to the most critical scenario. Therefore, the extreme arm unbalanced condition should be considered, since it represents the worst-case scenario for the arm currents. According to (17), the switch sizing current, $I_{\mathrm{sw,min}}^{\mathrm{VSC}}$, can be defined as:

$$I_{\mathrm{sw,min}}^{\mathrm{VSC}} = \frac{i_{\mathrm{arm}}^{\max}}{\sqrt{2}} k_{\mathrm{v}} = \left(\frac{3 + \sqrt{21}}{12\sqrt{2}} \right) i_{\mathrm{g,d}}^{\mathrm{r}} k_{\mathrm{v}}, \tag{22}$$

where the margin factor $k_{\mathrm{v}} > 1$ holds for possible grid voltage variations. Indeed, for the same active power exchanged, if the grid voltage decreases, the arm current rises proportionally. The switch sizing voltage, $V_{\mathrm{sw,min}}^{\mathrm{VSC}}$, equal to the maximum SM voltage, which depends on the characteristics of the integrated PV array and can be expressed as a function of $P_{\mathrm{ac}}^{\mathrm{r}}$ and $i_{\mathrm{g,d}}^{\mathrm{r}}$ as follows:

$$V_{\mathrm{sw,min}}^{\mathrm{VSC}} = V_{\mathrm{SM}}^{\mathrm{VSC,r}} k_{\mathrm{v}} k_{\mathrm{PV}}^{\mathrm{VSC}} = 8 \frac{P_{\mathrm{ac}}^{\mathrm{r}}}{N i_{\mathrm{g,d}}^{\mathrm{r}}} k_{\mathrm{v}} k_{\mathrm{PV}}^{\mathrm{VSC}}, \tag{23}$$

where $k_{\mathrm{PV}}^{\mathrm{VSC}}$ is defined as:

$$k_{\mathrm{PV}}^{\mathrm{VSC}} = \frac{V_{\mathrm{oc}}^{\max}(T_{\min})}{V_{\mathrm{mpp}}^{\min}(T_{\max})} > 1, \tag{24}$$

where $V_{\mathrm{mpp}}^{\min}(T_{\max})$ is the minimum MPP voltage, determined at minimum irradiance and at the maximum temperature at which the PV module should operate, whereas $V_{\mathrm{oc}}^{\max}(T_{\min})$ is the maximum SM operating voltage (i.e. the open-circuit voltage (OCV)) evaluated at maximum irradiance and minimum temperature. The factor $k_{\mathrm{PV}}^{\mathrm{VSC}}$ allows the converter arms to operate in the whole range (related to the ambient conditions) of the

integrated PV arrays. Hence, the semiconductor power rating $P_{\mathrm{sw}}^{\mathrm{MMVS}}$ is obtained by multiplying $V_{\mathrm{sw,min}}^{\mathrm{VSC}}$ and $I_{\mathrm{sw,min}}^{\mathrm{VSC}}$:

$$P_{\mathrm{sw}}^{\mathrm{MMVS}} = 8\frac{P_{\mathrm{ac}}^{\mathrm{r}}}{N i_{\mathrm{g,d}}^{\mathrm{r}}} k_{\mathrm{v}} k_{\mathrm{PV}}^{\mathrm{VSC}} \left(\frac{3+\sqrt{21}}{12\sqrt{2}}\right) i_{\mathrm{g,d}}^{\mathrm{r}} k_{\mathrm{v}} = \\ = \left(\frac{6+2\sqrt{21}}{3\sqrt{2}}\right) \frac{P_{\mathrm{ac}}^{\mathrm{r}}}{N} k_{\mathrm{v}}^2 k_{\mathrm{PV}}^{\mathrm{VSC}}. \tag{25}$$

Finally, considering (2) and (4), the overall converter semiconductor power rating, $P_{\mathrm{sw,tot}}^{\mathrm{MMVS}}$, computed considering the total number of switches of the MMVS, is given by:

$$P_{\mathrm{sw,tot}}^{\mathrm{MMVS}} = N_{\mathrm{switches}}^{\mathrm{MMVS}} P_{\mathrm{sw}}^{\mathrm{MMVS}} = \\ = 2\left(\frac{6+2\sqrt{21}}{3\sqrt{2}}\right) P_{\mathrm{ac}}^{\mathrm{r}} k_{\mathrm{v}}^2 k_{\mathrm{PV}}^{\mathrm{VSC}}. \tag{26}$$

It is important to highlight that the previous analysis does not account for the fact that the number of series and parallel-connected PV modules in the SMs is integer. Therefore, the actual values of the sizing voltage and current of the switches might be slightly different from the ones provided by the aforementioned formulas. Hence, the designer should verify a posteriori (i.e. considering the exact number of PV modules connected in series and in parallel in the SMs) that the voltage and current ratings of the chosen semiconductor match the design requirements.

4.2 | Current source MMC

The total capacitive energy of the current source MMC is stored by the SMs capacitors and the output capacitive filter. The scope of the SM capacitors is to smooth voltage ripples across the PV arrays, acting as an "energy buffer" and compensating power mismatches. The energy stored by the SM capacitors is:

$$E_{\mathrm{dc}} = \frac{M}{2} C_{\mathrm{dc}} {V_{\mathrm{SM}}^{\mathrm{CSC,r}}}^2, \tag{27}$$

where $V_{\mathrm{SM}}^{\mathrm{CSC,r}}$ is the rated SM voltage, which can be defined as:

$$V_{\mathrm{SM}}^{\mathrm{CSC,r}} = \frac{P_{\mathrm{SM}}^{\mathrm{r}}}{I_{\mathrm{dc}}^{\mathrm{r}}} = \frac{P_{\mathrm{ac}}^{\mathrm{r}}/M}{i_{\mathrm{g,d}}^{\mathrm{r}}/M} = \frac{P_{\mathrm{ac}}^{\mathrm{r}}}{i_{\mathrm{g,d}}^{\mathrm{r}}}. \tag{28}$$

In (28), the rated SM power was considered equal to $P_{\mathrm{SM}}^{\mathrm{r}} = P_{\mathrm{ac}}^{\mathrm{r}}/M$ and the rated SM DC current equal to $I_{\mathrm{dc}}^{\mathrm{r}} = i_{\mathrm{g,d}}^{\mathrm{r}}/M$. In fact, in this work, the phase-shift carrier PWM was considered and each SM operates, according to the irradiance condition, with unitary modulation index to extract its own maximum available power. Therefore, $i_{\mathrm{g,d}}^{\mathrm{r}}/M$ corresponds to $I_{\mathrm{dc}}^{\mathrm{r}}$.

The sizing of the SM capacitor C_{dc} can be determined under the assumption that $I_{\mathrm{dc}} \approx$ const and $R_{\mathrm{dc}} \approx 0$. The expression for C_{dc} is:

$$C_{\mathrm{dc}} = \frac{\Delta P}{f_{\mathrm{s}} V_{\mathrm{SM}}^{\mathrm{CSC,r}} \Delta V_{\mathrm{SM}}^{\mathrm{CSC,r}}} = \frac{\xi_{\mathrm{p}} P_{\mathrm{ac}}^{\mathrm{r}}}{M f_{\mathrm{s}} \xi_{\mathrm{sm,csc}}^{\mathrm{rip}} {V_{\mathrm{SM}}^{\mathrm{CSC,r}}}^2}, \tag{29}$$

where $\xi_{\mathrm{sm,csc}}^{\mathrm{rip}} \in (0,1]$ represents the voltage ripple for the rated SM voltage, while $\xi_{\mathrm{p}} \in (0,1]$ is the expected power mismatch between the power injected by the PV array and the SM output power. It is interesting to note that, compared to the voltage source MMC, due to the three-phase nature of the SMs, the SM capacitors are not subject to 100 Hz voltage oscillations, and they are sized to filter out the high-frequency component instead. Merging (27) with (28) and (29), it follows that:

$$E_{\mathrm{dc}} = \frac{M}{2} C_{\mathrm{dc}} {V_{\mathrm{SM}}^{\mathrm{CSC,r}}}^2 = \frac{\xi_{\mathrm{p}} P_{\mathrm{ac}}^{\mathrm{r}}}{2 f_{\mathrm{s}} \xi_{\mathrm{sm,csc}}^{\mathrm{rip}}}. \tag{30}$$

Considering instead the output filter capacitors, the energy stored by a wye-connected three-phase capacitor bank is:

$$E_{\mathrm{f}} = \frac{3}{2} C_{\mathrm{f}} {v_{\mathrm{g,d}}^{\mathrm{r}}}^2 = \frac{2}{3} C_{\mathrm{f}} \frac{{P_{\mathrm{ac}}^{\mathrm{r}}}^2}{{i_{\mathrm{g,d}}^{\mathrm{r}}}^2}. \tag{31}$$

The output capacitors aim at minimizing the output current ripple, by providing a low impedance path for the current harmonic component at the switching frequency. Therefore, neglecting the voltage drop on the grid impedance, their sizing is related to the allowed ripple of the rated grid current, $\Delta i_{\mathrm{g,d}}^{\mathrm{r}}$, and to the maximum allowed voltage variation across the capacitors, $\Delta v_{\mathrm{g,d}}^{\mathrm{r}}$. These can be both related to the rated grid voltage and current through two design parameters (the grid voltage and current ripple, that is, ξ_{vg} and ξ_{ig}, respectively), representing two degrees of freedom fixed by the designer. In light of these considerations, it follows that:

$$C_{\mathrm{f}} = \frac{\Delta i_{\mathrm{g,d}}^{\mathrm{r}}}{2\pi f_{\mathrm{s}} \Delta v_{\mathrm{g,d}}^{\mathrm{r}}} = \frac{\xi_{\mathrm{ig}} i_{\mathrm{g,d}}^{\mathrm{r}}}{2\pi f_{\mathrm{s}} \xi_{\mathrm{vg}} v_{\mathrm{g,d}}^{\mathrm{r}}} = \frac{2}{3} \frac{\xi_{\mathrm{ig}} P_{\mathrm{ac}}^{\mathrm{r}}}{2\pi f_{\mathrm{s}} \xi_{\mathrm{vg}} {v_{\mathrm{g,d}}^{\mathrm{r}}}^2}, \tag{32}$$

where $\xi_{\mathrm{ig}} \in (0,1]$ and $\xi_{\mathrm{vg}} \in (0,1]$. Merging (31) and (32), the final expression of E_{f} is:

$$E_{\mathrm{f}} = \frac{\xi_{\mathrm{ig}} P_{\mathrm{ac}}^{\mathrm{r}}}{2\pi f_{\mathrm{s}} \xi_{\mathrm{vg}}}. \tag{33}$$

Therefore, the overall capacitive energy stored by the current source MMC is computed as the sum of (30) and (33):

$$E_{\mathrm{c,csc}} = \frac{P_{\mathrm{ac}}^{\mathrm{r}}}{2\pi f_{\mathrm{s}}} \left(\frac{\xi_{\mathrm{p}} \pi}{\xi_{\mathrm{sm,csc}}^{\mathrm{rip}}} + \frac{\xi_{\mathrm{ig}}}{\xi_{\mathrm{vg}}}\right). \tag{34}$$

Concerning the total inductive energy stored in DC-side inductors, it is strictly related to the DC current of the SMs, I_{dc},

and it can be expressed as:

$$E_{\mathrm{l,csc}} = \frac{M}{2} L_{\mathrm{dc}} {I_{\mathrm{dc}}^{\mathrm{r}}}^2 = \frac{M}{2} L_{\mathrm{dc}} \left(\frac{i_{\mathrm{g,d}}^{\mathrm{r}}}{M} \right)^2. \tag{35}$$

The scope of the DC-side inductors is to suppress the high frequency ripple on the DC SM current, ΔI_{dc}, which equals:

$$\Delta I_{\mathrm{dc}} = \xi_{\mathrm{i,dc}}^{\mathrm{rip}} I_{\mathrm{dc}}^{\mathrm{r}} = \frac{\Delta V_{L\mathrm{dc}}}{L_{\mathrm{dc}} f_{\mathrm{s}}} \tag{36}$$

where $\xi_{\mathrm{i,dc}}^{\mathrm{rip}} \in (0, 1]$ represents the maximum allowed DC current ripple, and it is a degree of freedom fixed by the designer. Additionally, the maximum voltage ripple across the inductor, $\Delta V_{L\mathrm{dc}}$, is given by:

$$\Delta V_{L\mathrm{dc}} = \left| V_{\mathrm{SM}}^{\mathrm{CSC,r}} - \sqrt{3} v_{\mathrm{g,d}}^{\mathrm{r}} \right| = \left| \frac{P_{\mathrm{SM}}^{\mathrm{r}}}{I_{\mathrm{dc}}} - \sqrt{3} v_{\mathrm{g,d}}^{\mathrm{r}} \right| = \\ = \left| \frac{P_{\mathrm{ac}}^{\mathrm{r}}}{i_{\mathrm{g,d}}^{\mathrm{r}}} - \frac{2\sqrt{3} P_{\mathrm{ac}}^{\mathrm{r}}}{3 i_{\mathrm{g,d}}^{\mathrm{r}}} \right|. \tag{37}$$

Therefore, the DC-side inductors can be sized as:

$$L_{\mathrm{dc}} = \frac{\Delta V_{L\mathrm{dc}}}{\Delta I_{\mathrm{dc}} f_{\mathrm{s}}} = \frac{P_{\mathrm{ac}}^{\mathrm{r}} M}{\xi_{\mathrm{i,dc}}^{\mathrm{rip}} {i_{\mathrm{g,d}}^{\mathrm{r}}}^2 f_{\mathrm{s}}} \left| 1 - \frac{2\sqrt{3}}{3} \right|. \tag{38}$$

Lastly, the total inductive energy is given by:

$$E_{\mathrm{l,csc}} = \frac{P_{\mathrm{ac}}^{\mathrm{r}}}{2 \xi_{\mathrm{i,dc}}^{\mathrm{rip}} f_{\mathrm{s}}} \left| 1 - \frac{2\sqrt{3}}{3} \right|. \tag{39}$$

The semiconductor power rating is calculated separately for a MMCS-RB and a MMCS-NRB. In particular, only six IGBTs with RB capabilities are present in each SM for the MMCS-RB, while the MMCS-NRB requires using MOSFETs with an additional series diode providing the RB capability. For each SM of the MMCS-RB converter, the peak voltage applied to each RB-IGBT is the grid line-to-line voltage, which relates to the direct axis grid voltage as $\sqrt{3} v_{\mathrm{g,d}}^{\mathrm{r}}$. Therefore, considering appropriate margin factor, the switch sizing voltage, $V_{\mathrm{sw,min}}^{\mathrm{CSC}}$, is equal to:

$$V_{\mathrm{sw,min}}^{\mathrm{CSC}} = \sqrt{3} v_{\mathrm{g,d}}^{\mathrm{r}} k_{\mathrm{v}}. \tag{40}$$

Unlike voltage source MMCs, for current source MMCs, different levels of irradiance of the PV arrays directly affect only the value of the DC side current I_{dc} of each SM. Since each SM of the current source MMC operates independently from each other, the ratings of the semiconductors do not account for the presence of additional circulating currents. The worst case scenario occurs during the normal operation of the converters, in which, the RMS currents of the active switches and series reverse-blocking diodes are equal to $I_{\mathrm{dc}}^{\mathrm{r}} / \sqrt{3}$, independently from the modulation index [33]. Moreover, it is necessary to guarantee that the converter operates in boost mode, meaning that the DC-bus voltage of the SM is lower than $3 v_{\mathrm{g,d}}^{\mathrm{r}} / 2$. On the other hand, it is preferable to connect as many module as possible in series to limit their output current given the same power. In this way, power losses reduce. Therefore, the minimum sizing switch current, $I_{\mathrm{sw,min}}^{\mathrm{CSC}}$, is:

$$I_{\mathrm{sw,min}}^{\mathrm{CSC}} = \frac{I_{\mathrm{dc}}^{\mathrm{r}}}{\sqrt{3}} k_{\mathrm{PV}}^{\mathrm{CSC}} k_{\mathrm{v}} = \frac{i_{\mathrm{g,d}}^{\mathrm{r}}}{M\sqrt{3}} k_{\mathrm{PV}}^{\mathrm{CSC}} k_{\mathrm{v}}, \tag{41}$$

where $k_{\mathrm{PV}}^{\mathrm{CSC}}$ is defined as:

$$k_{\mathrm{PV}}^{\mathrm{CSC}} = \frac{V_{\mathrm{oc}}^{\max}(T_{\min})}{V_{\mathrm{mpp}}} > 1, \tag{42}$$

with V_{mpp} the MPP voltage of the PV module at standard test conditions. Similarly to $k_{\mathrm{PV}}^{\mathrm{VSC}}$, also for the current source MMC the factor $k_{\mathrm{PV}}^{\mathrm{CSC}}$ allows the converter SMs to operate in the whole range (related to the ambient conditions) of the integrated PV arrays.

Hence, the power semiconductor rating, yields:

$$P_{\mathrm{sw}}^{\mathrm{MMCS-RB}} = \sqrt{3} v_{\mathrm{g,d}}^{\mathrm{r}} \frac{I_{\mathrm{dc}}^{\mathrm{r}}}{\sqrt{3}} k_{\mathrm{PV}}^{\mathrm{CSC}} k_{\mathrm{v}}^2 = \frac{v_{\mathrm{g,d}}^{\mathrm{r}} i_{\mathrm{g,d}}^{\mathrm{r}}}{M} k_{\mathrm{PV}}^{\mathrm{CSC}} k_{\mathrm{v}}^2. \tag{43}$$

Merging (43) with (3), (4), and (7), the overall converter semiconductor power rating is given by:

$$P_{\mathrm{sw,tot}}^{\mathrm{MMCS-RB}} = \left(N_{\mathrm{switches}}^{\mathrm{MMCS-RB}} + N_{\mathrm{diodes}}^{\mathrm{MMCS-RB}} \right) P_{\mathrm{sw}}^{\mathrm{MMCS-RB}} = \\ = 4 P_{\mathrm{ac}}^{\mathrm{r}} k_{\mathrm{PV}}^{\mathrm{CSC}} k_{\mathrm{v}}^2. \tag{44}$$

Considering instead a MMCS-NRB converter, the power rating of the MOSFETs is computed again as in (44). However, also the rating of the RB diodes has to be accounted for. Due to the series connection, the current flowing into this component is the same one as the MOSFET. Regarding the voltage, the diode purpose is to provide the RB capability by blocking the line-to-line voltage; therefore, the peak voltage across this diode is also equal to $\sqrt{3} v_{\mathrm{g,d}}^{\mathrm{r}}$. Therefore, accounting for these considerations, it is possible to conclude that the diodes and the MOSFETs of a MMCS-NRB have the same rating. Thus, considering the MOSFETs with their series RB diode as a single component, the overall MMCS-NRB semiconductor power rating is expressed as:

$$P_{\mathrm{sw,tot}}^{\mathrm{MMCS\text{-}NRB}} = \left(N_{\mathrm{switches}}^{\mathrm{MMCS\text{-}NRB}} + N_{\mathrm{diodes}}^{\mathrm{MMCS\text{-}NRB}} \right) P_{\mathrm{sw}}^{\mathrm{MMCS\text{-}NRB}} = \\ = 2 P_{\mathrm{sw,tot}}^{\mathrm{MMCS-RB}} = 8 P_{\mathrm{ac}}^{\mathrm{r}} k_{\mathrm{PV}}^{\mathrm{CSC}} k_{\mathrm{v}}^2. \tag{45}$$

It is worth highlighting that, unlike voltage source MMCs, both the energy stored by the passive components and the power ratings of the semiconductors of current source MMCs do not depend on the irradiance conditions of the PV plant. Indeed, the operation of the converter is not affected by possible irradiance imbalances, as the SMs of the MMC can

operate independently without requiring additional circulating current components.

4.3 | Inductive and capacitive energy ratios

After obtaining the expressions of the total inductive and capacitive energy for both families of converters, their comparison is effectively performed by computing the ratios $E_{l,vsc}/E_{l,csc}$ and $E_{c,vsc}/E_{c,csc}$. Let us consider first the inductive energy. After performing all the necessary simplifications, it follows that:

$$\frac{E_{l,vsc}}{E_{l,csc}} = \frac{4\xi_{i,dc}^{rip}}{N\xi_{arm}^{rip}} \frac{\left(3+\sqrt{21}\right)}{\left|1-\frac{2\sqrt{3}}{3}\right|}. \tag{46}$$

It is possible to highlight that, supposing to fix the ripples on the DC and on the arm inductor currents, $\xi_{i,dc}^{rip}$ and ξ_{arm}^{rip}, respectively, equal to, for example, 0.2 (as a suitable design choice), then $E_{l,vsc}/E_{l,csc} \approx 196/N$. Hence, considering that in a voltage source MMC N is always multiple of six, it follows that voltage source MMCs store less inductive energy with respect to current source MMCs only when $N \geq 198$, which means that the number of levels of the two converters has to be higher than 77.

Let us now compute the capacitive energy ratio. The final expression becomes:

$$\frac{E_{c,vsc}}{E_{c,csc}} = m_f \frac{1}{2\xi_{sm,vsc}^{rip}\sqrt{(6-4\sqrt{3})\left(\xi_{sm,vsc}^{rip\,2}-4\right)}} \Bigg/ \left(\frac{\pi\xi_p}{\xi_{sm,csc}^{rip}} + \frac{\xi_{ig}}{\xi_{vg}}\right), \tag{47}$$

where $m_f = f_s/f$ is the frequency modulation index. In this case, there is no dependence on the structural characteristics of the two converters, that is, on the number of SMs. Considering to fix $\xi_{sm,vsc}^{rip}$, ξ_p, $\xi_{sm,csc}^{rip}$, ξ_{ig}, and ξ_{vg} equal to 0.2, the value of m_f for which the capacitive energy ratio equals one results $m_f \approx 3.2$. Therefore, it is possible to conclude that much more capacitive energy is stored in a voltage source MMC than in a current source MMC. Indeed, if $f_s = 10$ kHz and $f = 50$ Hz (i.e. $m_f = 200$), then, $\frac{E_{c,vsc}}{E_{c,csc}} \approx 63$.

4.4 | Semiconductor ratings ratios

Consider the expressions in (26), (44), and (45) for the semiconductor ratings of a MMVS, a MMCS-RB, and a MMCS-NRB converter, respectively. The same approach used for the total capacitive and inductive energy is also applied to compare these power ratings. To be more specific, the comparison involves computing two ratios, that is, $P_{sw}^{MMVS}/P_{sw}^{MMCS-RB}$ and $P_{sw}^{MMVS}/P_{sw}^{MMCS-NRB}$, assuming that both converters provide the same number of levels N_{lev} for the output voltage or current waveforms.

The ratio between the power ratings of the semiconductors for the MMVS and the MMCS-RB converter yields:

$$\frac{P_{sw,tot}^{MMVS}}{P_{sw,tot}^{MMCS-RB}} = \frac{\left(3\sqrt{2}+\sqrt{42}\right)}{6} \frac{k_{PV}^{VSC}}{k_{PV}^{CSC}}. \tag{48}$$

Hence, by fixing $k_{PV}^{VSC} = 1.2 \cdot k_{PV}^{CSC}$ (according to (24) and (42)), k_{PV}^{VSC} is always greater than k_{PV}^{CSC}), the overall power rating of the switches of the MMVS is roughly double that of the RB-IGBTs in an MMCS-RB converter.

Computing the same ratio for a MMVS and a MMCS-NRB converter realized using MOSFETs with series RB diodes gives:

$$\frac{P_{sw,tot}^{MMVS}}{P_{sw,tot}^{MMCS-NRB}} = \frac{\left(3+\sqrt{21}\right)}{6\sqrt{2}} \frac{k_{PV}^{VSC}}{k_{PV}^{CSC}}. \tag{49}$$

According to the considerations provided in Section 4.3, (49) results exactly equal to half of (48), since the power rating of the MOSFETs and series diodes of a MMCS-NRB current source converter are equal. Indeed, considering again $k_{PV}^{VSC} = 1.2 \cdot k_{PV}^{CSC}$, the overall power rating of the semiconductors of an MMVS is roughly the same as that of an MMCS-NRB.

It is once again worth noticing that these ratios do not depend on the topological characteristics of the MMCs, that is, on the number of SMs.

5 | CASE STUDY

In this section, a case study is presented to compare the number of components, regulators, total inductive and capacitive energy, and semiconductor devices power ratings between the two considered MMC topologies, that is, voltage and current source MMCs. Specifically, the current source MMC is considered to be realized using non-reverse-blocking devices (MMCS-NRB), and thus it requires additional series diodes. Eventually, the efficiency of the two converters is evaluated for both cases of uniform and non-homogeneous irradiance conditions.

The system consists of a 50 kW PV plant interfaced with a 400 V low-voltage grid. The number of levels for both MMCs is fixed at 7 and the switching frequency is set to $f_s = 10$ kHz. Additionally, the PV module specifically considered for this analysis is the JAM72S10 410/MR 410 W, produced by *JA Solar*. The PV temperature range was considered between 10 °C and 60 °C. The PV module parameters are listed in Table 3. Lastly, as for the previous considerations, the MMVS adopts phase-disposition pulse width modulation (PD-PWM) as a modulation scheme, while for the MMCS-NRB current source converter, phase-shift carrier PWM (PSC-PWM) is employed.

5.1 | Converters comparison

Table 1 presents the overall count of active and passive components required for the realization of both MMCs, along with

TABLE 1 Main converters quantities.

	MMVS		MMCS-NRB		Ratio
Quantity	**Value**	**Eq.**	**Value**	**Eq.**	**Value**
SMs	18	(2)	3	(3)	6
Switches + diodes	36+0	(4)	18+18	(4)	1
Inductors	6	–	3	(3)	2
Capacitors	18	(2)	6	$M+3$	3
PI regulators	14	–	9	$3M$	1.6
MPP trackers	18	(2)	3	(3)	6
Capacitive energy	207.5 J	(12)	3.3 J	(34)	≈ 63
Inductive energy	21.1 J	(21)	1.9 J	(39)	11.1
Semiconductor power rating	782.4 kW	(26)	720.0 kW	(45)	1.09

the total capacitive and inductive energy stored by the two converters, the number of PI regulators and MPP trackers, and the power ratings of the semiconductors. Additionally, the resulting ratios for all the evaluated quantities are computed. The following parameters are used for the computations: $k_{\mathrm{v}} = 1.2$, $\xi^{\mathrm{rip}}_{\mathrm{sm,vsc}}$, $\xi^{\mathrm{rip}}_{\mathrm{sm,csc}}$, $\xi^{\mathrm{rip}}_{\mathrm{arm}}$, $\xi^{\mathrm{rip}}_{\mathrm{i,dc}}$, ξ_{ig}, ξvg set to 0.2. Finally, according to the characteristics of the adopted PV module, $k^{\mathrm{VSC}}_{\mathrm{PV}}$ is determined to be 1.52, while $k^{\mathrm{CSC}}_{\mathrm{PV}} = 1.25$.

As evident, to achieve the same number of output levels, fewer SMs are required for the MMCS-NRB compared to the MMVS. However, the total number of semiconductor devices is the same for the two topologies. This is due to the necessity for the MMCS-NRB to add one RB diode for each switch. Regarding the passive components, the MMVS requires more elements, mainly due to the higher number of SMs, and the total energy stored in these components is much higher than that of the MMCS-NRB. Additionally, even though the number of semiconductor devices is the same, the components employed in the SMs are subject to different current and voltage values, leading to different semiconductor power ratings. The switch current ratings are lower for the MMCS-NRB compared to the MMVS; however, the MMVS structure allows reducing the voltage that the semiconductor devices have to withstand, as each SM is responsible for synthesizing only a portion of the total output voltage. Conversely, for the MMCS-NRB, due to the connection of the —which are in parallel with respect to the external grid—each semiconductor device (i.e. both active switches and RB diodes) must withstand the total line-to-line voltage at the connection point. By computing the semiconductor power ratings, it results that the MMVS semiconductor power rating is 9% higher than that of the MMCS-NRB. Finally, from a control perspective, the total number of PI regulators and MPP trackers is higher for the MMVS compared to the MMCS-NRB. The MMVS features a more distributed structure, allowing a broader subdivision of the whole PV plant, thus better managing the operation under irradiance imbalances. In contrast, it is more challenging to control, requiring several MPP trackers and additional regulation of the circulating current components. However, as visible from Figure 5, in the case of a higher number of output levels compared to 3, as defined for this case study, the number of PI regulators of the MMCS-NRB would be greater than that of the MMVS.

5.2 | Converters design and efficiency analysis

In order to assess the efficiency of the two MMCs, it is essential to initially determine the rated values of the grid current and voltage, as well as the number of PV modules integrated into each SM. These quantities need to be computed first in order to evaluate the adoptable passive components and semiconductor devices based on market availability. Consequently, it should be noted that the total number of components, the actual stored energy in the converter, and the power semiconductor ratings could slightly differ from the values obtained previously due to the discrete values of the components voltage and current ratings. However, this aspect does not impact the efficiency comparison between the two MMCs. Regarding the passive components, only the inductor losses were considered for the analysis.

5.2.1 | Converters design

Given the rated power of the PV system and the rated grid voltage, that is, 50 kW and 400 V, respectively, and assuming only active power injection into the grid, the rated values of the d components of the grid voltages and currents are:

$$\begin{cases} v^{\mathrm{r}}_{\mathrm{g,d}} = 326.6\ \mathrm{V} \\ i^{\mathrm{r}}_{\mathrm{g,d}} = 102.1\ \mathrm{A} \end{cases}. \tag{50}$$

For the MMVS, based on the grid requirements and the number of SMs per arm, that is, $N/6 = 3$, the number of series- and parallel-connected PV modules in each SM, $n^{\mathrm{MMVS}}_{\mathrm{PV,s}}$ and $n^{\mathrm{MMVS}}_{\mathrm{PV,p}}$, respectively, are determined as [34]:

$$\begin{cases} n^{\mathrm{MMVS}}_{\mathrm{PV,s}} = \mathrm{ceil}\left[\dfrac{12 v^{\mathrm{r}}_{\mathrm{g,d}} k_{\mathrm{V}}}{N V^{\min}_{\mathrm{mpp}}(T_{\max})}\right] = 8 \\ n^{\mathrm{MMVS}}_{\mathrm{PV,p}} = \mathrm{ceil}\left[\dfrac{P^{\mathrm{r}}_{\mathrm{ac}}}{N n^{\mathrm{MMVS}}_{\mathrm{PV,s}} P_{\mathrm{PV,mod}}}\right] = 1 \end{cases}, \tag{51}$$

where $P_{\mathrm{PV,mod}}$ is the rated power of a single PV module. The series-connected PV modules are determined to synthesize the required grid voltage (the DC voltage of each arm should be at least double of the peak value of the grid voltage), while the parallel-connected PV modules aim to achieve the rated power of the plant. Considering the integrated PV array in each SM and the maximum RMS value of the arm current, the power semiconductor device ratings for the MMVS are selected according

TABLE 2 Power semiconductors parameters.

Parameter	C3M0025075K1	E4M0045075J2	C4D40120H
V_{sw}	750 V	750 V	1200 V
I_{sw}	59 A	34 A	41 A
R_{on}	25 mΩ	45 mΩ	34.2 mΩ
E_{on}	0.144 mJ	0.073 mJ	–
E_{off}	0.224 mJ	0.013 mJ	–
V_{cc}	500 V	500 V	–
I_{cc}	33.5 A	17.6 A	–
Q_{rr}	372 nC	184 nC	0 C
$V_{F,d}$	–	–	3 V

to:

$$\begin{cases} V_{sw} > n_{PV,s}^{MMVS} \cdot V_{oc}^{max} = 417.0\ \text{V} \\ I_{sw} > I_{sw,min}^{VSC} = 54.7\ \text{A} \end{cases}, \tag{52}$$

where V_{sw} and I_{sw} are the rated voltage and current of the semiconductor switch, respectively. Therefore, considering the market offering, the MOSFET C3M0025075K1 (59 A-750 V) produced by *Wolfspeed* is selected. The main switch characteristics are listed in Table 2.

The converter arm inductors are evaluated using (20): its minimum required value is 1.7 mH. Considering the arm current, the inductor 195 Series of *Hammond Manufacturing* was selected. The inductors parameters are:

$$\begin{cases} L_{arm} = 2\ \text{mH} \\ R_{arm} = 8\ \text{m}\Omega \end{cases}. \tag{53}$$

For the MMCS-NRB, according to the total number of SMs, $M = 3$, the number of the series- and parallel-connected PV modules in each SM, $n_{PV,s}^{MMVS}$ and $n_{PV,p}^{MMVS}$, respectively, are:

$$\begin{cases} n_{PV,s}^{MMCS\text{-}NRB} = \text{floor}\left[\dfrac{3v_{g,d}^{r}}{2V_{oc}^{max}(T_{min})}\right] = 9 \\ n_{PV,p}^{MMCS\text{-}NRB} = \text{ceil}\left[\dfrac{P_{ac}^{r}}{Mn_{PV,s}^{MMCS\text{-}NRB}P_{PV,mod}}\right] = 5 \end{cases}. \tag{54}$$

This choice ensures that each SM properly operates in voltage boost mode. Additionally, given the total number of PV modules to integrate in each SM, it is preferable to connect as many of them in series rather than in parallel. This allows for the reduction of the current flowing into the DC side inductor and in the semiconductor devices, consequently decreasing the losses. According to the PV array in each SM, the power

TABLE 3 PV module JAM72S10 410/MR 410 W parameters.

Quantity	Values
Rated power $P_{PV,mod}$ @ 25°C	410 W
Open circuit voltage V_{oc} @ 25°C	50.12 V
MPP voltage V_{mpp} @ 25°C	41.88 V
Short circuit current I_{sc} @ 25°C	10.45 A
MPP current I_{mpp} @ 25°C	9.79 A
Maximum open circuit voltage V_{oc}^{max} (T_{min}) @ 10°C	52.16 V
Minimum MPP voltage V_{mpp}^{min} (T_{max}) @ 60°C	34.52 V

semiconductor device rating is selected according to:

$$\begin{cases} V_{sw} > V_{sw}^{CSC} = \sqrt{3}v_{g,d}^{r}k_{v} = 678.8\ \text{V} \\ I_{sw} > \dfrac{n_{PV,p}^{MMCS\text{-}NRB}P_{PV,mod}}{\sqrt{3}V_{mpp}}k_{v} = 33.9\ \text{A} \end{cases}, \tag{55}$$

where V_{mpp} is the MPP voltage of the PV module at standard test conditions, the scenario in which the highest current occurs since the maximum power is delivered by the SMs. It is worth noting that the actual power rating of the semiconductors differ from the one computed in (25) and (43), since the number of series and parallel-connected PV modules forming the integrated arrays are rounded to integers. In order to determine the RMS value of the current flowing in the switches, the DC-side current is considered. In the case of bypassing the SM, an opportune control strategy can be employed to alternatively short circuit the DC source with all three legs of the SM, thereby avoiding the situation where the full DC current flows through just one converter leg. Therefore, the worst condition occurs during normal operation, in which the RMS switch current is equal to $I_{dc}^{r}/\sqrt{3}$ [33]. Considering the required voltage and current ratings, also for this converter, the MOSFET E4M0045075J2 (34 A-750 V), produced by *Wolfspeed*, is selected. However, the MMCS-NRB requires also the series-diodes, which have the same rating as the MOSFET. Thus, the SiC diode C4D40120H produced by *Wolfspeed* is chosen. Its main parameters are also listed in Table 2.

The minimum required inductance of the SM inductor, designed according to (38), results in 1.1 mH. Therefore, according to the SM DC current, the inductor 195 Series of *Hammond Manufacturing* is selected, resulting in the following parameters:

$$\begin{cases} L_{dc} = 2\ \text{mH} \\ R_{dc} = 8\ \text{m}\Omega \end{cases}. \tag{56}$$

5.2.2 | Efficiency analysis

In order to assess the efficiency of the converters, the conduction and switching losses are computed first. The conduction

losses of the MMVS are:

$$P_{\text{cond}}^{\text{MMVS}} = \left(R_{\text{arm}} + \frac{N}{6}R_{\text{on}}^{\text{VSC}}\right)\frac{1}{T}\int_0^T \sum_{k=a,b,c}\left(i_{u,k}^2(t) + i_{l,k}^2(t)\right)dt, \tag{57}$$

where $R_{\text{on}}^{\text{VSC}}$ is the MOSFET on-state resistance, $i_{u,k}$ and $i_{l,k}$ are the upper and lower arm currents of the k-th phase, evaluated as in (14), and $T = 1/f$ is the fundamental period. It is worth noting that, since MOSFETs have bidirectional current flow capability, there is no need to differentiate which device is conducting. For each SM, the number of MOSFETs in the on-state is always equal to one.

The conduction losses of the MMCS-NRB are given by:

$$P_{\text{cond}}^{\text{MMCS-RB}} = \frac{6\left(R_{\text{on}}^{\text{CSC}} + R_{\text{on,d}}^{\text{CSC}}\right)}{T}\int_0^T \sum_{\substack{m=1\\ j=1,..,6}}^{M}\left(s_{m,j}(t)\cdot I_{\text{dc},m}(t)\right)^2 dt + \\ + \frac{6V_{\text{F,d}}}{T}\int_0^T \sum_{\substack{m=1\\ j=1,..,6}}^{M}\left(s_{m,j}(t)\cdot I_{\text{dc},m}(t)\right)dt + R_{\text{dc}}I_{\text{dc},m}(t)^2. \tag{58}$$

The first term represents the conduction losses of the MOSFETs, while the second term accounts for the conduction losses of the series-connected diodes. Specifically, $R_{\text{on}}^{\text{CSC}}$ is the on-state resistance of the semiconductor device employed for the MMCS-NRB, $R_{\text{on,d}}^{\text{CSC}}$ and $V_{\text{F,d}}$ are the on-state resistance and the forward voltage of the RB diode, respectively, while $s_{m,j}$ is the switching function of the j-th semiconductor device, and $I_{\text{dc},m}$ is the DC-side current of the m-th converter SM.

The switching losses are evaluated in the worst condition, that is, in case of hard switching transition, and are expressed as:

$$P_{\text{comm}} = \frac{V_{\text{SM}}\sum_{c=1}^{n_{\text{comm}}}|i_c|}{V_{\text{cc}}I_{\text{cc}}}\left(E_{\text{on}} + E_{off}\right)f + \\ + n_{\text{comm}}V_{\text{SM}}Q_{\text{rr}}f, \tag{59}$$

where n_{comm} is the total number of commutations occurring in one fundamental period in all the converter SMs, V_{SM} and i_c are the voltage and current at the commutation instants. Additionally, Q_{rr} is the reverse recovery charge of the diode, and I_{cc} and V_{cc} are the operating voltage and current, defined by the datasheet, at which the turn-on and turn-off switch energies, that is, E_{off} and E_{on}, respectively, are provided in the datasheet. For the sake of simplicity, equation (59) was reported in a general form, without distinguishing the formulae for the two converters. However, it is worth noting that, V_{SM} is equal to $V_{\text{SM}}^{\text{VSC}}$ or $V_{\text{SM}}^{\text{CSC}}$ for the MMVS or MMCS-RB, respectively, and, all the semiconductor device parameters, should be defined according to device adopted for the considered converter.

The converters efficiencies were evaluated under homogeneous and non-homogeneous irradiance condition fixing the ambient temperature at 25°C. Even though, according to the sizing of the PV arrays as in (51) and (54), the maximum output powers result 59.0 kW and 55.4 kW for the MMVS and the MMCS-NRB, respectively, the numerical simulation were limited to 50 kW, which is the rated power of the converters. The simulation results for the first scenario are presented in Figure 6. Specifically, the PV plant irradiance was varied from 100 W/m^2 to 1000 W/m^2. Conversely, Figure 7 shows the results for the non-homogeneous irradiance condition. In this case, the worst condition in terms of power losses for both converters was considered. For the MMVS, the scenario described in (15) was evaluated. Consequently, three arms are exposed to the minimum irradiance condition, that is, 100 W/m^2, while the others vary uniformly up to 1000 W/m^2. On the other hand, for the MMCS-RB, the worst condition occurs when two SMs are irradiated at the minimum, while the remaining one varies uniformly up to 1000 W/m^2. Analyzing Figure 6a under uniform irradiance conditions, it is evident that the MMVS is more efficient than the MMCS-NRB across the entire operating range of the two converters. For both converters, conduction losses predominate over switching losses (Figures 6b and 6c). In the MMVS, the RMS current of the switch is equal to half of the injected grid current, that is, $\frac{i_{\text{g,d}}^r}{2\sqrt{2}}$. For the MMCS-NRB, according to the considered modulation technique, the RMS value of the individual semiconductor device is $\frac{i_{\text{g,d}}^r}{3\sqrt{3}}$, while its average value is $\frac{i_{\text{g,d}}^r}{9}$. Therefore, in the analyzed power range and considering the equivalent converter resistances, the conduction losses of the MMCS-NRB are more significant.

Figure 7 shows the results obtained under non-uniform irradiance conditions. In this situation, the power range of the converters is different since the worst condition in terms of efficiency occurs in different scenarios. For the MMVS, the highest losses are experienced when half of the arms operate at the minimum irradiation level and the others at the maximum possible, while for the MMCS-NRB, it occurs when one SM operates at the minimum irradiation level while the others operate at the maximum possible. Examining Figure 7a, it can be noted that, in this case as well, the MMVS is more efficient than the MMCS-NRB. The discrepancy between the converter efficiencies is attributed to the higher conduction losses of the MMCS-NRB, as illustrated in Figure 7b. Switching losses are comparable and not significant for both converters, as depicted in Figure 7c.

Moreover, it can be noted that the MMVS experiences lower efficiency compared to the homogeneous irradiance scenario. To operate each arm at the maximum power point, additional circulating currents must be injected into the converter. This is evident, as the same amount of output power can be injected into the grid with varying efficiencies according to the irradiance scenario. For instance, 20 kW under homogeneous conditions are injected into the grid with 98.9% efficiency, while under non-homogeneous condition the efficiency reduces to 97.1%, for the same output power. In contrast, the MMCS-NRB allows independent control of each SM, enabling them to inject their own maximum power individually. Consequently, the efficiency of the MMCS-NRB remains around 98–97% for every operating condition.

To summarize, for the considered case study, the MMVS shows greater efficiency compared to the MMCS-NRB under both homogeneous and non-homogeneous conditions.

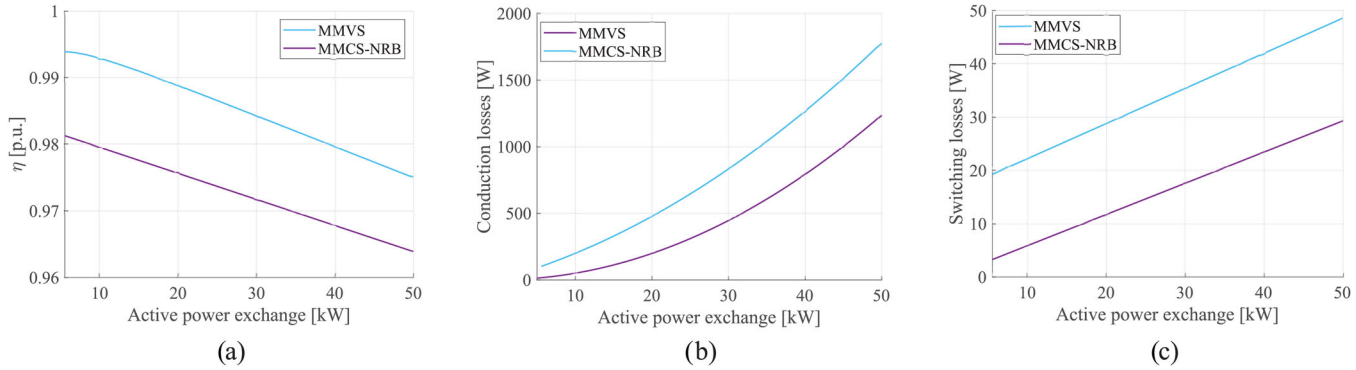

FIGURE 6 Uniform irradiance condition. (a) converters efficiency; (b) conduction losses; (c) switching losses.

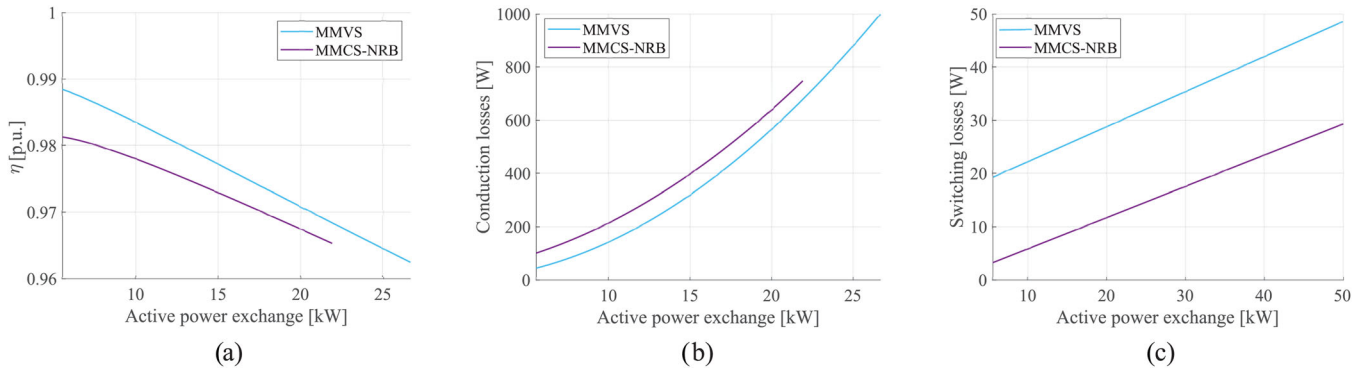

FIGURE 7 Non-homogeneous irradiance condition. (a) converters efficiency; (b) conduction losses; (c) switching losses.

However, it is worth pointing out that the efficiency evaluation strongly depends on the choice of semiconductor devices. To achieve a fair comparison, components from the same manufacturer have been chosen. However, different results may be obtained by adopting other available market solutions.

6 | CONCLUSIONS

This article presents a comprehensive comparison between two grid connected MMC topologies - a voltage source MMC and a current source MMC - for PV integration.

Assuming that the two converters have the same power rating, switching frequency and number of levels of the output voltage or current waveforms, this work firstly shows the results of a structural comparison, performed by counting how many active and passive elements are required for the realization of the two MMCs. In general, it is observed that current source MMCs require less SMs and thus also less active and passive components, for the same number of levels. This results from the different nature of the converters SMs: indeed, while the SMs of a current source MMC have three phase nature, the ones of a voltage source MMC are only able to modify the voltage levels of each phase. Concerning instead the control complexity, voltage source MMCs perform better than their current source counterparts, providing better DMPPT capability with a reduced control complexity.

The second part of this article highlights the comparison between the total energy stored by all the inductive and capacitive components of the two MMCs under analysis, as well as the comparison between the power ratings of the semiconductor devices. Voltage source MMCs store much more capacitive energy than current source MMCs. Moreover, the comparison shows that this energy is not depending on the structural characteristics of the two converters. Concerning instead the energy stored by the magnetics, again current source MMCs store less energy than voltage source MMCs, unless for very high number of levels. About the power rating of the semiconductors, considering the overall power accounting for all power electronics devices of the two converters, it results that voltage source MMCs and current source MMCs realized using MOSFETs with series diode for providing the RB capability have approximately the same global semiconductors power rating. On the other hand, in comparison to a current source MMC realized with RB-IGBTs, the overall semiconductors power rating of a voltage source MMC is roughly doubled.

Eventually, an efficiency comparison between the two converters is presented, as part of a case study regarding the grid integration of a 50 kW PV plant, considering both homogeneous and non-homogeneous irradiance conditions. More in detail, for what concerns the operation under non-homogeneous irradiance of the PV plant, the worst case scenario - in terms of losses - is considered, for both MMC topologies. It has to be highlighted that the efficiency compari-

TABLE 4 Comparison scores.

Quantity	MMVS Score	MMCS-NRB Score	MMCS-RB Score
Switches + diodes	5	5	8
Inductors	6	4	4
Capacitors	3	7	7
PI regulators	7	3	3
MPP trackers	8	2	2
Capacitive energy	1	10	10
Inductive energy	2	9	9
Semiconductor power rating	5	6	9
Average score:	**5**	**6**	**7**

son strongly depends on the choice of the components required for the realization of the converters. Therefore, to allow a fair comparison, the same inductors and active switches produced by the same manufacturers were chosen, according to the market availability and the sizing requirements of the components. The comparison results indicate that voltage source MMCs are more efficient than current source MMCs under both homogeneous and non-homogeneous irradiance conditions. Moreover, while the efficiency of current source MMCs remains relatively unchanged under both conditions, the opposite is true for voltage source MMCs. Indeed, the efficiency is sensibly different under homogeneous or non-homogeneous irradiance of the PV plant. More in detail, the efficiency decreases in case of partial shading of the PV arrays. This results from the presence of strong circulating current components, which are required to enable balanced operation of voltage source MMCs under heavy irradiance imbalances, thus increasing the power losses. Finally, for what concerns the efficiency computation of current source MMCs, the use of MOSFETs with series RB diodes is considered, in spite of using RB IGBTs. However, in case these latter active components are chosen, the formulas to employ in the calculations are not different. Indeed, even if the series diode and the active switch are integrated within the same package, datasheets of RB IGBTs expressively show the characteristics of the two devices as if the two were separate.

Eventually, to quantitatively highlight the outcomes of the analysis performed in this work, a score was assigned to the two converters. These scores account for the structural characteristics (i.e. the number of switches, diodes, inductors, and capacitors), as well as the control complexity and MPP tracking capabilities (i.e. the number of PI regulators and MPP trackers). Additionally, the scores consider the energy perspective (i.e. the energy stored by inductors and capacitors and the overall semiconductor power ratings of the two MMCs). However, no score was assigned to the efficiency, as it is strongly dependent on the specifications of the case study and the specific characteristics of the electrical components (i.e. inductors, capacitors, and power semiconductors) chosen for the converters. The scores are reported in Table 4, considering a voltage source MMC, as well as both MMCS-NRB and MMCS-RB converters. They range from 1 to 10, with 1 indicating "worse" and 10 indicating "optimal." On average, the current source MMC received a higher score than its voltage source counterpart. Despite lacking DMPPT capabilities and exhibiting higher control complexity (i.e. requiring more PI regulators for the same number of levels), current source MMCs can be built using capacitors, inductors, and power semiconductor devices with lower energy and power ratings. Moreover, when comparing the MMCS-NRB converter with the MMCS-RB, the latter scored better on average due to the reduced semiconductor count, which also has a lower power rating. It is important to highlight that these average scores have been obtained by weighting each single score in the same way. However, different weights could be assigned to each score, thus leading to different average results. The choice of these weighting factors is devolved to the power electronics designer, depending on the requirements and characteristics of the specific application.

AUTHOR CONTRIBUTIONS

Marzio Barresi: Conceptualization; data curation; formal analysis; investigation; methodology; software; validation; visualization; writing—original draft; writing—review & editing. **Luigi Piegari**: Funding acquisition; project administration; resources; supervision; writing—review & editing. **Riccardo Scalabrin**: Conceptualization; data curation; formal analysis; investigation; methodology; software; validation; visualization; writing—original draft; writing—review & editing.

CONFLICT OF INTEREST STATEMENT

The authors declare no conflicts of interest.

DATA AVAILABILITY STATEMENT

Data sharing not applicable to this article as no datasets were generated or analysed during the current study.

ORCID

Riccardo Scalabrin https://orcid.org/0009-0008-8964-4203

REFERENCES

1. REN21: Renewables 2023—Global Status Report. https://www.ren21.net/gsr-2023/
2. Shafiullah, M., Ahmed, S.D., Al-Sulaiman, F.A.: Grid integration challenges and solution strategies for solar pv systems: A review. IEEE Access 10, 52 233–52 257 (2022)
3. Bhavani, M, Vijaybhaskar Reddy, K., Mahesh, K., Saravanan, S.: Impact of variation of solar irradiance and temperature on the inverter output for grid connected photo voltaic (pv) system at different climate conditions. Mater. Today: Proc. 80, 2101–2108 (2023). https://www.sciencedirect.com/science/article/pii/S2214785321044758
4. Motahhir, S., El Hammoumi, A., El Ghzizal, A.: The most used mppt algorithms: Review and the suitable low-cost embedded board for each algorithm. J. Cleaner Prod. 246, 118983 (2020). https://www.sciencedirect.com/science/article/pii/S0959652619338533
5. Libo, W., Zhengming, Z., Jianzheng, L.: A single-stage three-phase grid-connected photovoltaic system with modified mppt method and reactive power compensation. IEEE Trans. Energy Convers. 22(4), 881–886 (2007)
6. Rabiul Islam, M., Mahfuz-Ur-Rahman, A.M., Muttaqi, K.M., Sutanto, D.: State-of-the-art of the medium-voltage power converter technologies for grid integration of solar photovoltaic power plants. IEEE Trans. Energy Convers. 34(1), 372–384 (2019)

7. Chen, K., Tian, S., Cheng, Y., Bai, L.: An improved mppt controller for photovoltaic system under partial shading condition. IEEE Trans. Sustainable Energy 5(3), 978–985 (2014)
8. Elsanabary, A.I., Konstantinou, G., Mekhilef, S., Townsend, C.D., Seyedmahmoudian, M., Stojcevski, A.: Medium voltage large-scale grid-connected photovoltaic systems using cascaded h-bridge and modular multilevel converters: A review. IEEE Access 8, 223 686–223 699 (2020)
9. Priya, M., Ponnambalam, P., Muralikumar, K.: Modular-multilevel converter topologies and applications-a review. IET Power Electron. 12(2), 170–183 (2019)
10. Dehghani Tafti, H., Maswood, A.I., Lim, Z., Ooi, G.H.P., Raj, P.H.: Npc photovoltaic grid-connected inverter with ride-through capability under grid faults. In: 2015 IEEE 11th International Conference on Power Electronics and Drive Systems, pp. 518–523. IEEE, Piscataway (2015)
11. Hammami, M., Ricco, M., Ruderman, A., Grandi, G.: Three-phase three-level flying capacitor pv generation system with an embedded ripple correlation control mppt algorithm. Electronics 8(2), 118 (2019)
12. Villanueva, E., Correa, P., Rodriguez, J., Pacas, M.: Control of a single-phase cascaded h-bridge multilevel inverter for grid-connected photovoltaic systems. IEEE Trans. Ind. Electron. 56(11), 4399–4406 (2009)
13. Kumar, A., Verma, V.: Performance enhancement of single-phase grid-connected pv system under partial shading using cascaded multilevel converter. IEEE Trans. Ind. Appl. 54(3), 2665–2676 (2018)
14. Sochor, P., Akagi, H.: Theoretical and experimental comparison between phase-shifted pwm and level-shifted pwm in a modular multilevel sdbc inverter for utility-scale photovoltaic applications. IEEE Trans. Ind. Appl. 53(5), 4695–4707 (2017)
15. Yu, Y., Konstantinou, G., Hredzak, B., Agelidis, V.G.: Power balance optimization of cascaded h-bridge multilevel converters for large-scale photovoltaic integration. IEEE Trans. Power Electron. 31(2), 1108–1120 (2016)
16. Amaral, F.V., Parreiras, T.M., Lobato, G.C., Machado, A.A.P., Pires, I.A., de Jesus Cardoso Filho, B.: Operation of a grid-tied cascaded multilevel converter based on a forward solid-state transformer under unbalanced pv power generation. IEEE Trans. Ind. Appl. 54(5), 5493–5503 (2018)
17. Rong, F., Gong, X., Huang, S.: A novel grid-connected pv system based on mmc to get the maximum power under partial shading conditions. IEEE Trans. Power Electron. 32(6), 4320–4333 (2017)
18. Barcellona, S., Barresi, M., Piegari, L.: Mmc-based pv three-phase system with distributed mppt. IEEE Trans. Energy Convers. 37(3), 1567–1578 (2022)
19. Rivera, S., Wu, B., Lizana, R., Kouro, S., Perez, M., Rodriguez, J.: Modular multilevel converter for large-scale multistring photovoltaic energy conversion system. In: 2013 IEEE Energy Conversion Congress and Exposition, pp. 1941–1946. IEEE, Piscataway (2013)
20. Bayat, H., Yazdani, A.: A power mismatch elimination strategy for an mmc-based photovoltaic system. IEEE Trans. Energy Convers. 33(3), 1519–1528 (2018)
21. Sahan, B., Vergara, A.N., Henze, N., Engler, A., Zacharias, P.: A single-stage pv module integrated converter based on a low-power current-source inverter. IEEE Trans. Ind. Electron. 55(7), 2602–2609 (2008)
22. Xing, L., Wei, Q., Li, Y.: A practical current source inverter-based high-power medium-voltage pv system. IEEE Trans. Power Electron. 38(2), 2617–2625 (2023)
23. Lorenzani, E., Immovilli, F., Migliazza, G., Frigieri, M., Bianchini, C., Davoli, M.: Csi7: A modified three-phase current-source inverter for modular photovoltaic applications. IEEE Trans. Ind. Electron. 64(7), 5449–5459 (2017)
24. Singh, A., Mirafzal, B.: An efficient grid-connected three-phase single-stage boost current source inverter. IEEE Power Energy Technol. Syst. J. 6(3), 142–151 (2019)
25. Torres, M., Espinoza, J., Morán, L., Rohten, J., Melín, P.: Integration of a large-scale photovoltaic plant using a multilevel converter topology and virtual synchronous generator control. In: 2014 IEEE 23rd International Symposium on Industrial Electronics (ISIE), pp. 2620–2624. IEEE, Piscataway (2014)
26. Dash, P.P., Kazerani, M.: Dynamic modeling and performance analysis of a grid-connected current-source inverter-based photovoltaic system. IEEE Trans. Sustainable Energy 2(4), 443–450 (2011)
27. Barresi, M., Piegari, L., Scalabrin, R., di Milano, P.: Voltage and current source modular multilevel converters comparison for pv integration. In: 2023 International Conference on Clean Electrical Power (ICCEP), pp. 273–281. IEEE, Piscataway (2023)
28. Debnath, S., Qin, J., Bahrani, B., Saeedifard, M., Barbosa, P.: Operation, control, and applications of the modular multilevel converter: A review. IEEE Trans. Power Electron. 30(1), 37–53 (2015)
29. Huber, J., Kolar, J.W.: Monolithic bidirectional power transistors. IEEE Power Electron. Mag. 10(1), 28–38 (2023)
30. Akagi, H., Kanazawa, Y., Fujita, K., Nabae, A.: Generalized theory of the instantaneous reactive power and its application. Trans. Inst. Electr. Eng. Japan B 103(7), 483–490 (1983)
31. Spier, D.W., Prieto-Araujo, E., Lyu, H., He, J., Li, B., Gomis-Bellmunt, O.: Optimization-based methodology to design the mmc's sub-module capacitors. IEEE Trans. Power Delivery 38(1), 475–486 (2023)
32. Barcellona, S., Barresi, M., Piegari, L.: A sizing procedure for the dc-side capacitor of a three-phase modular multilevel converter. Energies 16(19), 6945 (2023)
33. Barresi, M., De Simone, D., Piegari, L., Scalabrin, R.: Novel current source converter for integrating multiple energy storage systems. Energies 17(11), 2495 (2024). https://www.mdpi.com/1996-1073/17/11/2495
34. Barcellona, S., Barresi, M., Piegari, L.: Mmc-based pv single-phase system with distributed mppt. Energies 13(15), 3964 (2020)

How to cite this article: Barresi, M., Piegari, L., Scalabrin, R.: Comprehensive assessment of voltage and current source PV-based modular multilevel converters. IET Renew. Power Gener. 1–17 (2024). https://doi.org/10.1049/rpg2.13099

APPENDIX: DERIVATION OF THE MAXIMUM ARM CURRENT OF THE MMVS

The MMVS arm current, $i_{\mathrm{arm},k}$, is defined as:

$$i_{\mathrm{arm},k} = \pm\frac{i_{\mathrm{g},k}}{2} + i_{\mathrm{circ},k}. \tag{A1}$$

where $i_{\mathrm{g},k}$ is the output converter current and depends on the power exchanged with the grid, while $i_{\mathrm{circ},k}$ is the circulating current and depends on the internal converter power imbalances. The grid component is given by:

$$i_{\mathrm{g,d}} = \frac{2}{3}\frac{P_{\mathrm{ac}}}{v^{\mathrm{r}}_{\mathrm{g,d}}}. \tag{A2}$$

Additionally, to derive the maximum value of the arm current the influence of the circulating current components should be considered. Depending on the internal converter power mismatches, specific components are generated. In particular, the AC component is generated to make each converter arm work at its own maximum power point, while the DC component to balance the power injected into the grid. For each k-th phase, the AC circulating current, $i^{\mathrm{ac}}_{\mathrm{circ},k}$, is related to the instantaneous differential power, $p_{\mathrm{d},k}$, of the converter arms as [32]:

$$p_{\mathrm{d,k}} = \frac{p_{\mathrm{u},k} - p_{\mathrm{l},k}}{2} \simeq v^{\mathrm{r}}_{\mathrm{g,d}} i^{\mathrm{ac}}_{\mathrm{circ},k} = v^{\mathrm{r}}_{\mathrm{ph,d}} i^{\mathrm{ac}}_{\mathrm{circ},k}, \tag{A3}$$

where $v^{r}_{ph,d}$ is the voltage component generated by the MMVS responsible for exchanging power with the grid, and $p_{u,k}$ and $p_{l,k}$ are the upper and lower instantaneous power, respectively. In (A3), assuming neglecting the voltage drops on the converter impedances, the voltage component $v^{r}_{ph,d}$ can be considered equal to $v^{r}_{g,d}$. By defining the AC circulating currents over time as function of the positive and negative sequences, it can be written:

$$i^{ac}_{circ,k} = I^{ac}_{circ,+}\cos\left(\omega t - \varphi_{+} - \frac{2\pi(m-1)}{3}\right) + I^{ac}_{circ,-}\cos\left(\omega t - \varphi_{-} + \frac{2\pi(m-1)}{3}\right), \tag{A4}$$

where $m = 1, 2, 3$ for $k = a, b, c$, respectively, $I^{ac}_{circ,+}$ and $I^{ac}_{circ,-}$ are the amplitudes of the positive and negative sequences, respectively, φ_{+} and φ_{-} are the phase displacement of the positive and negative sequences of the AC circulating currents with respect to $v^{r}_{g,d}$. Considering (A4) and (A3), the active and reactive differential powers can be retrieved as:

$$\begin{cases} P_{d,k} = \dfrac{v^{r}_{g,d}}{2}\left[I^{ac}_{circ,+}\cos\left(\varphi_{+}\right) + I^{ac}_{circ,-}\cos\left(\varphi_{-} + \dfrac{2\pi(m-1)}{3}\right)\right] \\ Q_{d,k} = -\dfrac{v^{r}_{g,d}}{2}\left[I^{ac}_{circ,+}\sin\left(\varphi_{+}\right) + I^{ac}_{circ,-}\sin\left(\varphi_{-} + \dfrac{2\pi(m-1)}{3}\right)\right]. \end{cases} \tag{A5}$$

The active arm differential powers $P_{d,k}$ depend on the arm irradiance conditions, while $Q_{d,k}$ represents a degree of freedom for the adopted control strategy. In order to maximize the efficiency, it is possible to impose $\sum Q_{d,k} = 0$. Consequently, the relationship between $P_{d,k}$ and the sequence phasors of the AC circulating currents can be derived as:

$$\begin{bmatrix} I^{ac}_{circ,+}\cos\left(\varphi_{+}\right) \\ I^{ac}_{circ,+}\sin\left(\varphi_{+}\right) \\ I^{ac}_{circ,-}\cos\left(\varphi_{-}\right) \\ I^{ac}_{circ,-} - \sin\left(\varphi_{-}\right) \end{bmatrix} = \frac{2}{3v^{r}_{g,d}}\begin{bmatrix} 1 & 1 & 1 \\ 0 & 0 & 0 \\ 2 & -1 & -1 \\ 0 & \sqrt{3} & -\sqrt{3} \end{bmatrix}\begin{bmatrix} P_{d,a} \\ P_{d,b} \\ P_{d,c} \end{bmatrix}. \tag{A6}$$

Lastly, the phasors of the phase AC circulating currents, $\bar{I}^{ac}_{circ,k}$, and the active differential powers, $P_{d,k}$, are linked by:

$$\begin{bmatrix} \bar{I}^{ac}_{circ,a} \\ \bar{I}^{ac}_{circ,b} \\ \bar{I}^{ac}_{circ,c} \end{bmatrix} = \frac{2}{3v^{r}_{g,d}}\begin{bmatrix} 3 & \sqrt{3}e^{j\frac{\pi}{2}} & \sqrt{3}e^{-j\frac{\pi}{2}} \\ \sqrt{3}e^{j\frac{5}{6}\pi} & 3e^{-j\frac{2}{3}\pi} & \sqrt{3}e^{-j\frac{\pi}{6}} \\ \sqrt{3}e^{-j\frac{5}{6}\pi} & \sqrt{3}e^{j\frac{\pi}{6}} & 3e^{j\frac{2}{3}\pi} \end{bmatrix}\begin{bmatrix} P_{d,a} \\ P_{d,b} \\ P_{d,c} \end{bmatrix}. \tag{A7}$$

For each k-th phase, the DC circulating current, $i^{dc}_{circ,k}$, is related to the active sum power, $P_{s,k}$, as:

$$i^{dc}_{circ,k} = \frac{\sum_{k} P_{s,k}/3 - P_{s,k}}{2v^{r}_{g,d}}, \tag{A8}$$

where $P_{s,k} = \left(P_{u,k} + P_{l,k}\right)$, with $P_{u,k}$ and $P_{l,k}$ the upper and lower active power, respectively. In (A8), the term at the denominator represents the converter DC-bus voltage. Neglecting the internal voltage drops, it can be defined as the two times the peak value of the grid voltage. This value is the minimum DC arm voltage required to synthesize the reference voltage.

In order to determine the maximum value of the arm current, (A1) should be evaluated for different power exchanged with the grid and internal converter power imbalances. For the sake of simplicity, it was considered to exchange only active power with grid. Assuming that the output power of one arm, $P_{u,k}$ or $P_{l,k}$, are defined in the following range $(0, P^{r}_{ac}/6]$, the absolute value of (A1) can be written as:

$$\left|i_{arm,k}\right| = \left|\frac{2\sum_{k}\left(P_{u,k} + P_{l,k}\right)}{3v^{r}_{g,d}} + i^{ac}_{circ,k} + i^{dc}_{circ,k}\right|, \tag{A9}$$

and evaluated, considering all the possible output arm powers, in order to find the maximum arm current value, that is, i^{max}_{circ}.

By numerically solving (A9), it is possible to demonstrate that the highest arm current occurs when:

$$\begin{cases} P_{d,k} = P_{u,k} - P_{l,k} = \pm P^{r}_{ac}/6 & k \in a, b, c \\ P_{d,y} = P_{d,z} = -P_{d,k} & y \neq k, z \neq y, \neq k \\ P_{s,a} = P_{s,b} = P_{s,c} & \\ \sum_{k=a,b,c}\left(P_{u,k} + P_{l,k}\right) = P^{r}_{ac}/2 & \end{cases}. \tag{A10}$$

In this scenario, only power imbalances among the arms are present, therefore only the AC component of the circulating current is considered. Instead, since all the leg powers, $P_{s,k}$, are equal each others, the DC circulating components are zero as deducible from (A8). Additionally, due to the internal arm imbalances defined in (A10), the output converter results half of the rated one, that is, $P^{r}_{ac}/2$. By substituting (A10) in (A7) and considering (A2), the maximum value of the AC circulating component can be retrieved. It is given by:

$$i^{max}_{circ} = \frac{\sqrt{21}i^{r}_{g,d}}{12}. \tag{A11}$$

Then, considering the output converter power, that is, $P^{r}_{ac}/2$, the maximum value of the arm current yields:

$$i^{max}_{arm} = \left|\frac{i_{g,d}}{2}\right| + i^{max}_{circ} = \frac{i^{r}_{g,d}}{4} + \frac{\sqrt{21}i^{r}_{g,d}}{12}. \tag{A12}$$